MATERIALS CHEMISTRY
FRONTIERS

REVIEW

View Article Online
View Journal | View Issue

Cite this: *Mater. Chem. Front.*, 2024, **8**, 82

The role of organic spacers in 2D/3D hybrid perovskite solar cells

Yu Zou, Yuping Gao and Yongsheng Liu *

Received 29th June 2023,
Accepted 18th September 2023

DOI: 10.1039/d3qm00726j

rsc.li/frontiers-materials

The long-term stability of three-dimensional (3D) perovskite solar cells (PSCs) has become the major challenge for their commercial applications. To solve this problem, the development of 2D/3D hybrid perovskites by incorporating bulky organic spacers into 3D perovskite films has been proposed as an efficient strategy to combine the high efficiency of 3D PSCs and high stability of 2D PSCs. In this review, we present the structure of 3D and 2D perovskite materials, discuss the transformation process from 3D to 2D perovskite, and summarize the key organic spacers used in 2D/3D PSCs. Most importantly, based on the appropriate selection of functional groups in organic spacers, we highlight the role of organic spacers in the fabrication process and formation mechanism of different types of 2D/3D perovskite heterojunctions including the bulk incorporation model, surface treatment model, and bulk incorporation and surface treatment coexisting model as well as other feasible models.

1. Introduction

The power conversion efficiency (PCE) of three-dimensional (3D) organic–inorganic metal hybrid perovskite solar cells (PSCs) has increased sharply from the initial 3.8%[1] to a certified value of 26.1%[2] in the past decade. Moreover, many studies have demonstrated that the excellent PCE of 3D PSCs primarily stems from the unique properties of perovskite materials, such as high carrier mobility,[3] high absorption coefficient,[4] long carrier lifetime[5,6] and low exciton binding energy.[7] These optoelectronic characteristics make perovskite materials outstanding light absorbers for the next generation of photovoltaic devices. However, despite the ultrahigh PCE of state-of-the-art PSCs, which is comparable to that of silicon-based solar cells, long-term stability remains a major challenge for commercialization due to issues such as moisture[8] and oxygen[9] attack, heat stress,[10] light soaking[11] and ion migration.[12]

In comparison, low dimensional perovskites, especially 2D perovskites consisting of 2D phases and quasi-2D phases, have been proven to be more durable than 3D perovskites due to the incorporation of bulky and hydrophobic organic spacers.[13] In 2014, Smith *et al.* demonstrated Ruddlesden–Popper (RP) type 2D PSCs by introducing a phenylethylammonium (PEA) organic spacer.[14] Although the corresponding photovoltaic device exhibited a low PCE of 4.73%, the layered structure of 2D perovskite contributed to the formation of high-quality films that exhibited greater moisture resistance compared to the 3D $MAPbI_3$ (MA refers to methylammonium) film. Consequently, researchers began to devote significant efforts to the study of 2D PSCs and subsequently developed various organic spacers.[15–18] However, even though 2D perovskites demonstrate enhanced resilience to heat and humidity, the PCE of 2D PSCs still lags behind that of state-of-the-art 3D PSCs.[19]

To combine the high efficiency of 3D PSCs with superior stability of 2D PSCs, a dimensional engineering strategy has been proposed and developed. Through dimensional engineering, 2D/3D hybrid heterojunctions can be formed at different positions, wherein 3D perovskites ensure a wider absorption range for achieving high efficiency, while 2D perovskites guarantee that the device will not degrade rapidly under severe conditions. In addition to improving device stability, the construction of 2D/3D heterojunctions is also helpful in energy level regulation, ion migration suppression, defect passivation and residual stress release.[20] Generally, 2D/3D heterojunctions with the aforementioned high performance primarily fall into three types: (1) arranged in the bulk of 3D perovskite (referred to as the bulk incorporation model), (2) located on the top of 3D perovskite (referred to as the surface treatment model), and (3) situated both in the bulk and on the top of 3D perovskite (referred to as the bulk incorporation and surface treatment coexisting model).

However, despite the development of many organic spacers for constructing 2D/3D heterojunctions, a clear summary of the role of different types of organic spacers in the preparation process of these 2D/3D perovskites is still lacking. In this review, we first introduce the structures of 3D and 2D perovskite materials and explain the transformation process from 3D to 2D perovskite. Subsequently, we summarize the primary

The Centre of Nanoscale Science and Technology and Key Laboratory of Functional Polymer Materials, Institute of Polymer Chemistry, College of Chemistry and Renewable Energy Conversion and Storage Center (RECAST), Nankai University, Tianjin 300071, China. E-mail: liuys@nankai.edu.cn

organic spacers that have been used in reported 2D/3D PSCs so far and further analyze their effects on the photoelectric performance of devices. Finally, based on the appropriate selection of functional groups in organic spacers, we mainly focus on the role of organic spacers in the fabrication process and formation mechanism of various 2D/3D perovskite heterojunctions, including the bulk incorporation model, surface treatment model, bulk incorporation and surface treatment coexisting model, and other feasible models.

2. Structures of 3D and 2D perovskites

2.1. Structure of 3D perovskite

To gain a deeper understanding of the properties of perovskite materials, it is crucial to delve into their structures. Conventional perovskite materials are generally defined as a series of compounds with the formula of ABX_3. In this formula, the A site typically represents a monovalent cation, such as $CH_3NH_3^+$ (MA^+), $NH{=}CHNH_3^+$ (FA^+) and Cs^+. The B site usually denotes a divalent metal cation (Pb^{2+}, Sn^{2+}), while X site refers to halogen ions including Cl^-, Br^-, and I^-.[21] Within the perovskite framework, B site ions coordinate with X site ions to form a $[BX_6]^{4-}$ octahedron, in which the B site ions reside in the center of the octahedron and the X site ions occupy the apex positions. These $[BX_6]^{4-}$ octahedrons are further interconnected by vertices, extending into 3D space. Meanwhile, A site cations occupy the vacant space within the network formed by the $[BX_6]^{4-}$ octahedrons (Fig. 1).[22]

2.2. Structure of 2D perovskite

The tolerance factor (t) is often used to account for octahedral distortions in the crystal structure of perovskite to predict the 3D to 2D transition, in which t is defined by the following Goldschmidt's formula:[23]

$$t = \frac{R_A + R_X}{\sqrt{2}(R_B + R_X)}$$

The archetypal 3D perovskites have t values in the range of $0.8 < t < 1.1$. When the A site cations become too large to fit well within the $[BX_6]^{4-}$ octahedral cavity, the initial cubic structure of the 3D perovskite could transform into a layered 2D structure to maintain energy stability, thus leading to the deviation from the above range. Therefore, based on the arrangement of the 3D perovskite unit cells, 2D perovskites can be classified into (100), (110) and (111) orientations, where large organic spacers separate the inorganic layered $[BX_6]^{4-}$ octahedron and tightly connect the different layers through hydrogen bonding and van der Waals forces.[24] Depending on the types of organic spacers, 2D perovskite can be categorized into three main classifications: RP phase, Dion–Jacobson (DJ) phase, and alternating cations in the interlayer-space (ACI) phase (Fig. 1). These are expressed as $A'_2A_{n-1}B_nX_{3n+1}$, $A''A_{n-1}B_nX_{3n+1}$ and $A'''AB_nX_{3n+1}$, respectively. Here, A' represents monovalent organic cations like PEA and butylammonium (BA), A'' denotes a divalent organic cation, and A''' typically refers to guanidinium (GA). In the case of ACI perovskite, the large GA spacer and small A cations are arranged in the spacer layer, exhibiting the dual characteristics of RP and DJ structures. The value of n signifies the number of inorganic layers or the metal-halide frameworks located between the organic spacer layers.[25]

2.3. Organic spacer cations

2D perovskite materials offer significant advantages in terms of environmental stability. However, the presence of large organic spacers in the structure hinders the migration of photogenerated carriers and increases the exciton binding energy, ultimately leading to inferior photovoltaic performance of devices.[26] Therefore, the selection of effective organic spacers, while ensuring the high environmental stability of 2D perovskite and excellent photovoltaic performance of 3D perovskites, has emerged as a research focus for the development of efficient 2D/3D PSCs. In pursuit of this goal, scholars have conducted a series of investigations encompassing the

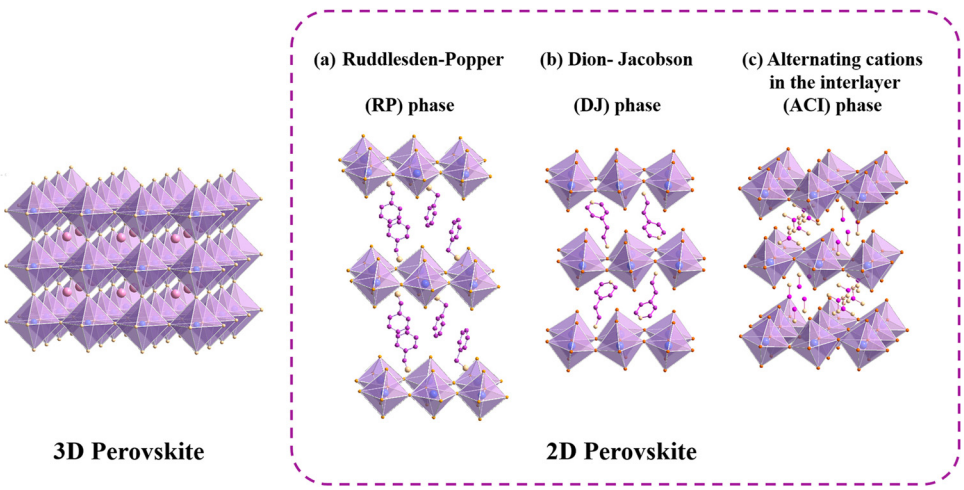

Fig. 1 Representative structures for 3D perovskite and 2D perovskite of the RP phase (a), DJ phase (b) and ACI phase (c).

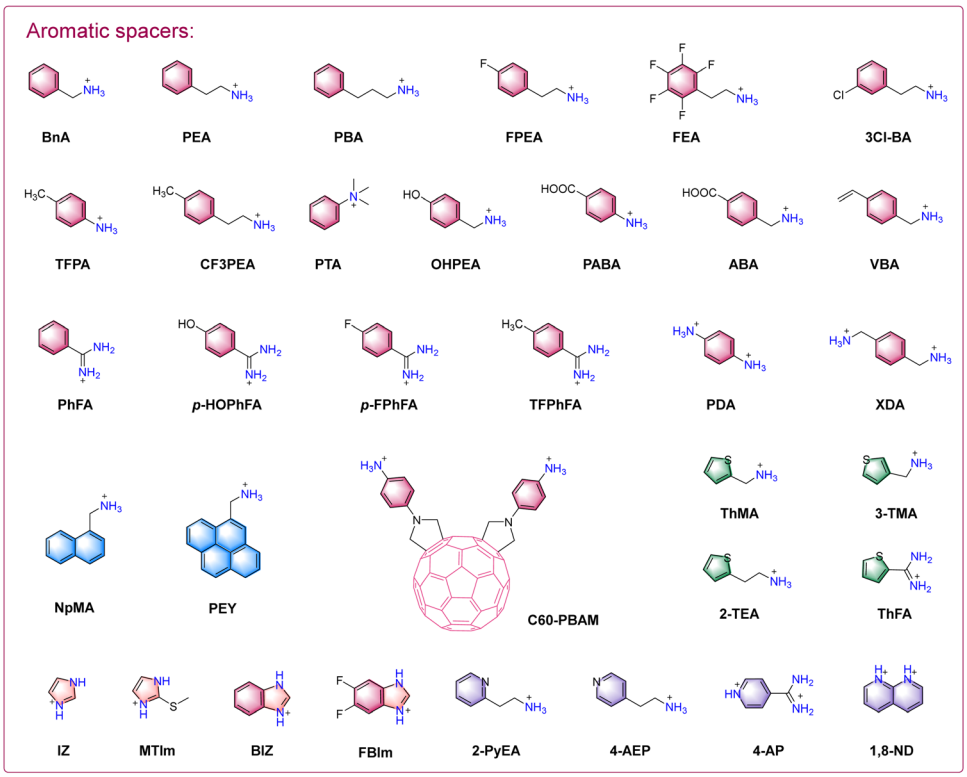

Fig. 2 Representative aromatic spacers for 2D/3D hybrid PSCs.

regulation of organic spacers, optimization of surface morphology and orientation, and the development of a diverse range of organic spacers (Fig. 2 and 3).[20]

3. 2D/3D heterojunctions in mixed dimensional perovskite solar cells

Mixed dimensional 2D/3D perovskite films can be fabricated through two common processes: bulk incorporation[27–31] and surface treatment.[32–35] In the bulk incorporation method, small amounts of large organic ammonium salts or 2D perovskite seed crystals are added to the 3D perovskite precursor. This allows for the growth of highly crystalline and the large grained 2D/3D perovskite with favorable out-of-plane layer orientation.[27,31] On the other hand, in surface treatment, 2D perovskite is formed *in situ* on the deposited 3D perovskite film by spin-coating a solution containing bulky organic ammonium salts[36] or 2D perovskite seed crystals.[34] Some researchers have also explored alternative methods such as evaporating bulky organic ammonium salts on the top of 3D perovskite films[37,38] or hot-pressing 2D perovskite films onto 3D perovskite films to create 2D/3D heterojunctions.[34] The performance enhancement achieved through the formation of a thin mixed 2D/3D heterojunction at the interface between the perovskite layer and the hole transport layer can be attributed to surface defect passivation, accelerated charge extraction, and the introduction of hydrophobic spacers to enhance humidity stability.

Based on the aforementioned statements, the main types of 2D/3D heterojunctions are illustrated in Fig. 4 as follows: (1) 2D/3D heterojunctions generated in the bulk of 3D perovskite films, causing the bulk incorporation model; (2) 2D/3D heterojunctions formed on the surface of 3D perovskites, leading to the surface treatment model; and (3) 2D/3D heterojunctions arranged on both the surface and bulk of 3D perovskite, resulting in the bulk incorporation and surface treatment coexisting model. We will analyze these structures and the role of large organic spacers in each structure in detail in the following discussion.

3.1. Bulk incorporation model

3.1.1. Aromatic spacers. In 2018, Ho-Baillie *et al.* reported the benefits of incorporating phenethylamine iodide salt (PEAI) into the $(FAPbI_3)_{0.85}(MAPbBr_3)_{0.15}$ perovskite and demonstrated the presence of a higher-band-gap PEA-based quasi-2D perovskite at grain boundaries using Kelvin probe force microscopy (KPFM).[39] After performing measurements in dark mode, the contact potential difference (CPD) at grain boundaries (CPD_{GB}) and in the grain interior (CBD_{GI}) were determined and the averaged differences of CPD_{GB} and CBD_{GI} were calculated. Notably, the value of 'CPD_{GB} − CBD_{GI}' in the film with 4.5% PEAI (−44 mV) was lower than that without PEAI (−13 mV), indicating a change in the electronic properties of the grain boundaries due to the formation of a quasi-2D phase at the grain boundaries. Additionally, in the same year, Yang *et al.* developed a fabrication technique for the pure α-phase $FAPbI_3$

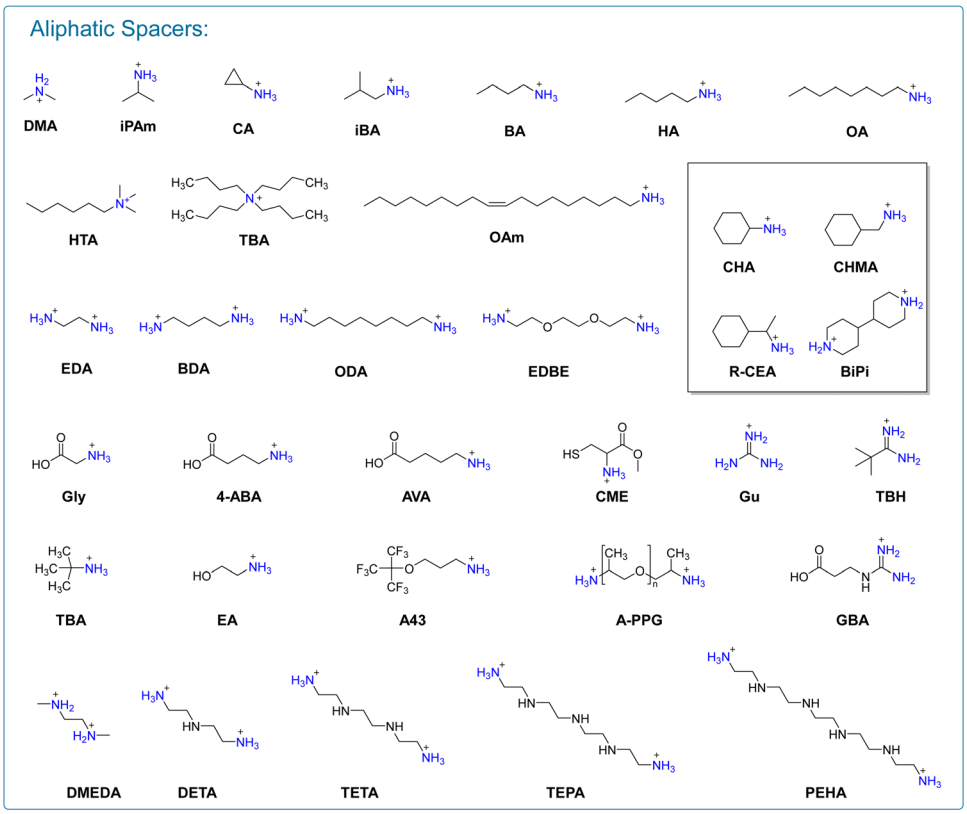

Fig. 3 Representative aliphatic and alicyclic spacers for 2D/3D hybrid PSCs.

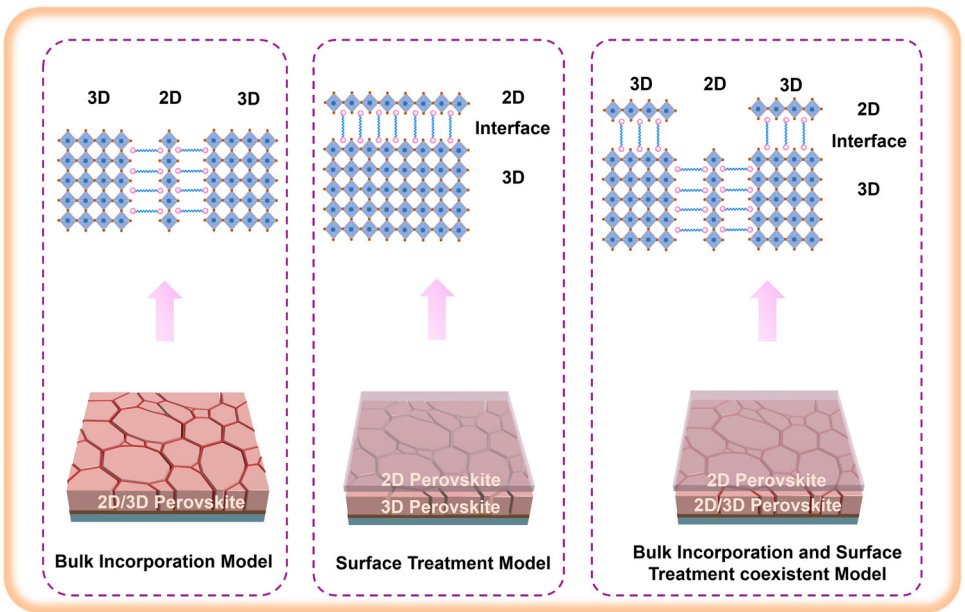

Fig. 4 Schematic diagram of the bulk incorporation model, surface treatment model, and bulk incorporation and surface treatment coexisting model.

perovskite by incorporating PEA_2PbI_4 2D perovskite seed crystals into the precursor solution.[28] In this process, 2D PEA_2PbI_4 passivated the defective grain boundaries of the 3D perovskite through aromatic rings and longer alkyl chains, resulting in a significantly improved hydrophobic property of the film. Furthermore, the 3D perovskite and PEA_2PbI_4 exhibited type I band alignment, which reduced charge recombination and facilitated charge separation and collection. Meanwhile, 2D

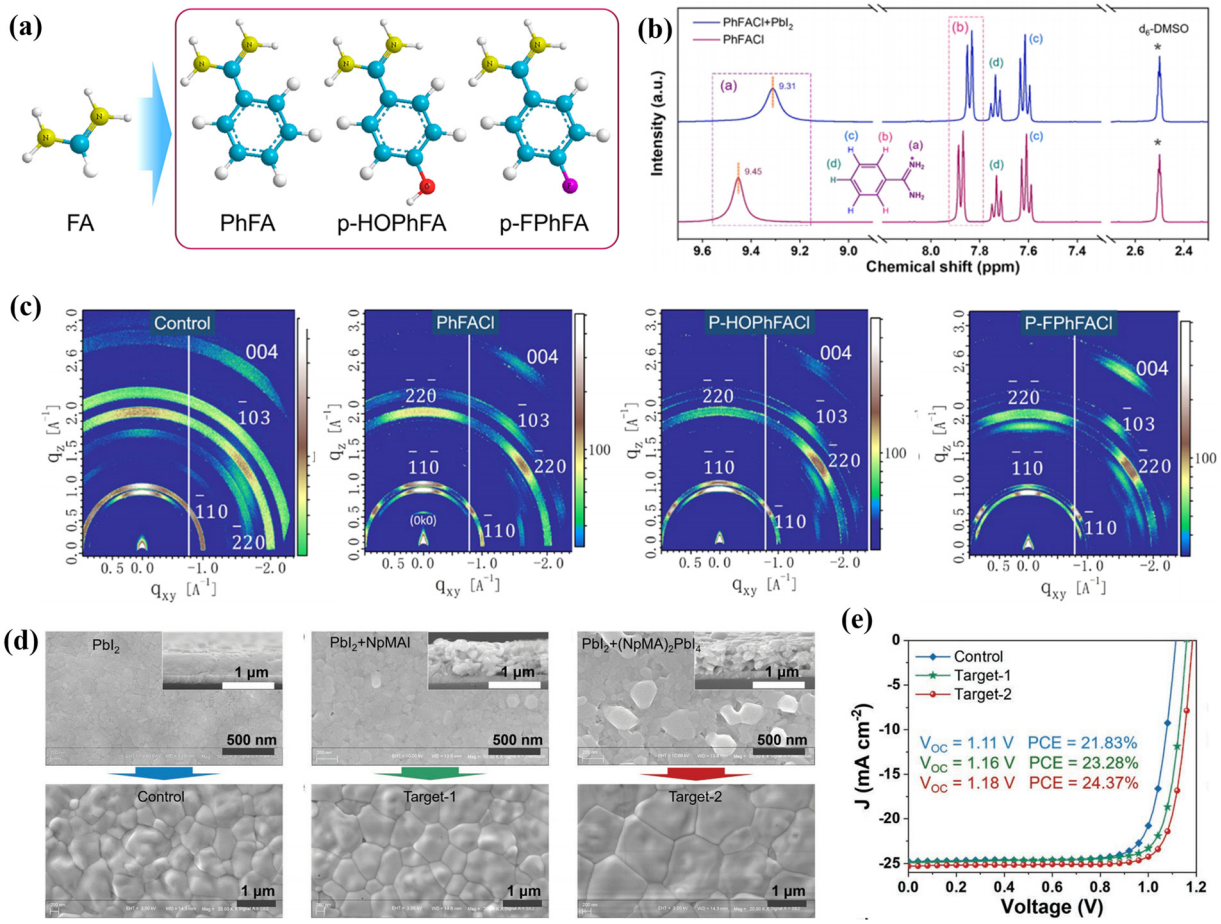

Fig. 5 (a) Chemical structures of spacer cations FA, PhFA, *p*-HOPhFA, and *p*-FPhFA. (b) ^{1}H NMR spectra of pristine PhFACl and mixed PhFACl/PbI_2. (c) GIWAX patterns of the control, PhFACl-, *p*-HOPhFACl-, and *p*-FPhFACl-based perovskite films. Reproduced with permission.[40] Copyright 2021, American Chemical Society. (d) Top-views and cross-sectional SEM images of pristine, NpMAI-modified and $(NpMA)_2PbI_4$-modified PbI_2 films and SEM images of the corresponding perovskite films. (e) *J*–*V* curves of the pristine, NpMAI-modified and $(NpMA)_2PbI_4$-modified devices. Reproduced with permission.[41] Copyright 2022, John Wiley & Sons, Inc.

perovskite regions at grain boundaries experienced a downward band bending under illumination, creating a high-potential barrier for holes and resulting in superior PL lifetime and photovoltaic performance.

In 2021, Liu *et al.* reported for the first time a class of aromatic formamidinium (ArFA) salts, which included benzamidine hydrochloride (PhFACl), 4-hydroxybenzamidinium hydrochloride (*p*-HOPhFACl), and 4-fluorobenzamidinium hydrochloride (*p*-FPhFACl), for 2D/3D hybrid PSCs (Fig. 5a).[40] As shown in Fig. 5b, the ^{1}H NMR spectra revealed strong NH···I hydrogen-bonding interactions between the iodide anions in the corner-sharing $[PbI_6]^{4-}$ octahedron layers and the ammonium fragment of organic spacers. The crystallographic quality and orientation of the perovskite crystals were confirmed using grazing-incidence wide-angle X-ray scattering (GIWAX). In contrast to the diffraction rings observed in the pristine film, the sharp and distinct Bragg spots in the ArFA films (Fig. 5c) suggested that the incorporation of ArFA spacers led to a preferred vertical orientation of the crystal with respect to the substrate. As a result, the optimized PhFA-based 2D/3D PSC exhibited a champion PCE of 23.36% with a high short-circuit current density (J_{SC}) of 24.67 mA cm^{-2}, an increased open-circuit voltage (V_{OC}) of 1.16 V and a notable fill factor (FF) of 81.54%.

In addition to the spacers with a single aromatic ring, multiple-ring aromatic spacers such as naphthyl-[41] and pyrenyl-based spacers[42] have also been applied in bulk 2D/3D PSCs. In 2022, Liu *et al.* reported the crystal growth regulation of 2D/3D perovskite films through a two-step spin-coating method by using 1-naphthalenemethylammonium iodide (NpMAI) or 2D perovskite $(NpMA)_2PbI_4$ as seed crystals in PbI_2 precursor solution.[41] They found that the pristine PbI_2 film showed a dense film morphology, while the PbI_2 film incorporated small quantity of $(NpMA)_2PbI_4$ or NpMAI, showing a mesoporous morphology, especially for the $(NpMA)_2PbI_4$ incorporated film. This mesoporous morphology benefitted the penetration and reaction of organic salts with PbI_2 in the second deposition step, resulting in a higher quality perovskite film with large grain size (Fig. 5d). Moreover, the application of $(NpMA)_2PbI_4$ seed doping can not only improve the crystallinity

of the perovskite film but also prolong the lifetime of charge carriers, thereby leading to a better photovoltaic performance of devices. Finally, the 2D/3D hybrid films with $(NpMA)_2PbI_4$ 2D perovskite exhibited a superior PCE of 24.37%, higher than that of the NpMAI-modified film (23.28%) and the control one (21.83%) (Fig. 5e). For pyrenyl-based spacers, 1-(ammonium acetyl)pyrene (PEY) was proposed to fabricate $MAPbI_3$-based 2D/3D perovskite by Hayase's group in 2018.[42] They demonstrated the enhancement of ultraviolet irradiation and oxygen stability due to the large functional organic pyrene group with high humidity resistance and strong absorption in the ultraviolet region.

Furthermore, the spacers based on heterocyclic rings such as thiophene and pyridine can also regulate the crystal arrangement and orientation through π–π interactions as well as hydrogen bonding interactions. In 2019, Liu *et al.* demonstrated highly efficient and stable 2D/3D hybrid PSCs using 2-thiophenemethylammonium (ThMA) as a spacer.[43] ThMA could partially insert into the 3D perovskite crystal lattice and form 2D perovskite phases, which aligned perpendicular to the substrate as confirmed by XRD and GIWAX measurements. Additionally, the introduction of a large ThMA spacer inhibited ion migration and improved the overall hydrophobic performance of 2D/3D films, leading to enhanced humidity stability in atmospheric environments. Remarkably, the ThMA spacer-based 2D/3D PSCs exhibited significantly improved performance, including a large V_{OC} of 1.16 V, a J_{SC} of 22.8 mA cm^{-2}, and a very notable FF of 81.0%, resulting in an impressive PCE of 21.49%. In contrast to benzene-based spacers, the pyridine ring possesses a lone electron pair on the N atom, allowing pyridine to partially replace DMSO by coordinating with Pb^{2+}.[44] Moreover, the weak alkalinity of N atoms in the pyridine unit enables the interaction between the pyridine ring with an amino terminal group and the $[PbI_6]^{4-}$ framework, ultimately forming DJ-type 2D perovskite.[30] Recently, Zhao *et al.* conducted a detailed investigation of the crystallization dynamics of 2D/3D hybrid perovskite by designing a 2D/3D heterojunction based on the $FAPbI_3$ 3D perovskite and DJ-type $(4AP)PbI_4$ 2D perovskite (4AP = 4-amidinopyridine).[30] As shown in Fig. 6a and b, the FA-rich α phase perovskite rapidly crystalized on the film's surface after dropping the anti-solvent, resulting in a sharp increase in PL intensity. Subsequently, the entrapped DMSO solvent volatilized from the bulk film during the annealing process, causing the surface perovskite to dissolve and recrystallize leading to a gradual decrease in PL intensity. Eventually, the evaporation of DMSO caused volume collapse of the internal perovskite, resulting in void formation at grain boundaries. In contrast, the addition of $(4AP)PbI_4$ 2D perovskite could slow down the nucleation and growth process of FA-rich α phase 3D perovskite, and the presence of $(4AP)PbI_4$ provided a skeleton that aided in the hetero-nucleation of 3D perovskite and filled the voids at grain boundaries caused by DMSO evaporation, resulting in more uniform and larger grains. Through this method, the 2D/

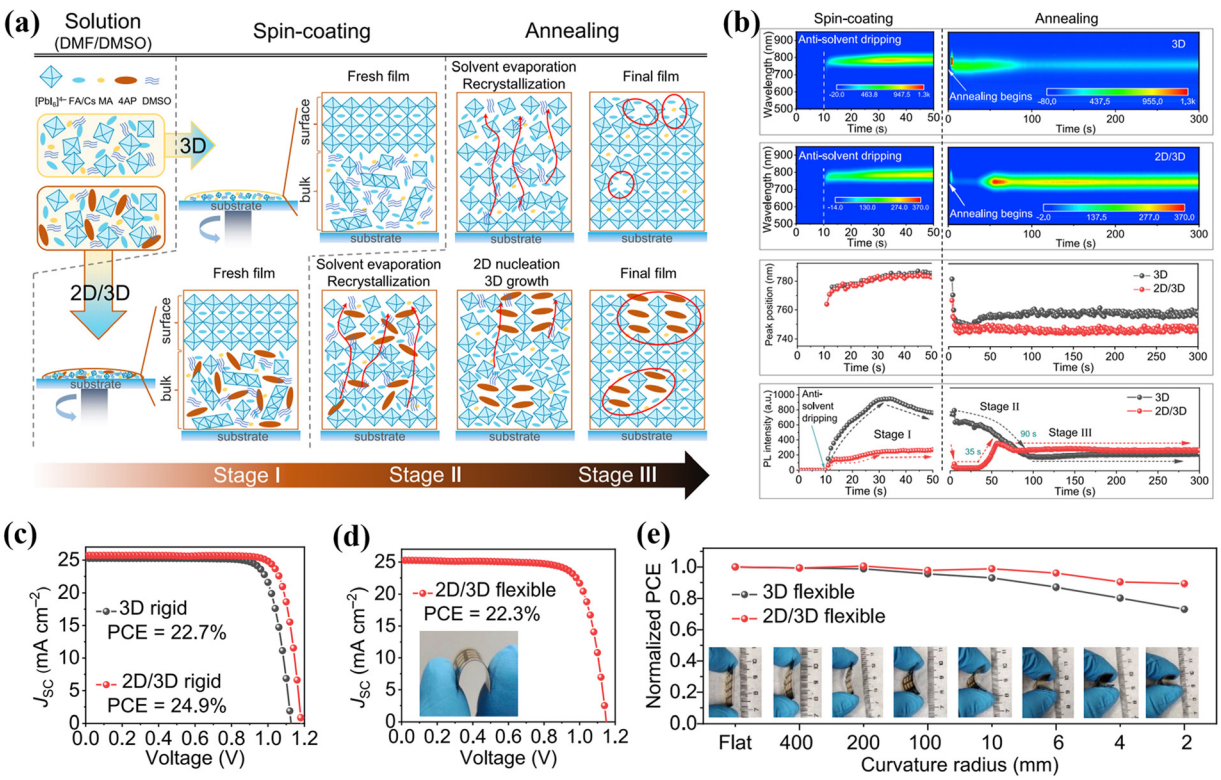

Fig. 6 (a) Schematic illustration of the crystallization mechanism of 4-AP modified perovskite films. (b) *In situ* PL measurements for the formation kinetics of perovskite films. *J*–*V* curves of rigid solar cells(c) and flexible solar cell (d). (e) Normalized PCE with curvature from flat to *R* = 2 mm. Reproduced with permission.[30] Copyright 2023, Elsevier.

3D films achieved a PCE of 24.9% in a rigid device and a PCE of 22.3% in a flexible device, with the PCE achieved by rigid device setting a record for 2D/3D hybrid PSCs to date (Fig. 6c–e).

3.1.2. Aliphatic spacers. Among aliphatic molecules, BA is a classical organic spacer commonly used to fabricate RP type 2D perovskites,[45–47] suggesting its potential for outstanding performance in 2D/3D perovskite systems. In 2017, Snaith *et al.* introduced BA spacer into a mixed-cation and mixed-halide $FA_{0.83}Cs_{0.17}Pb(I_yBr_{1-y})_3$ 3D perovskite.[27] Notably, plate-like 2D perovskites were observed to intersperse between highly orientated 3D perovskite grains, significantly enhancing crystallinity and suppressing non-radiative charge recombination through the formation of a classical type-I heterojunction (Fig. 7a–c). The device based on $BA_{0.09}(FA_{0.83}Cs_{0.17})_{0.91}Pb(I_{0.6}Br_{0.4})_3$ with a wide band gap of 1.72 eV achieved an optimized PCE of 17.2%, while the device utilizing the $BA_{0.05}(FA_{0.83}Cs_{0.17})_{0.95}Pb(I_{0.8}Br_{0.2})_3$ perovskite with a narrow band gap of 1.62 eV as the photoactive layer demonstrated a champion PCE of 20.6%. In 2021, Seok *et al.* found that the chemical reaction between the isopropyl alcohol (IPA) solvent and methylammonium chloride (MACl) in the precursor would generate isopropylammonium cations ($iPAmH^+$) in a two-step spin-coating process. Furthermore, $iPAmH^+$ could also be generated by adding IPA directly to the precursor in a one-step spin-coating process, where $iPAmH^+$ played a role in stabilizing the α-phase $FAPbI_3$.[48] Based on these findings, they directly added 15 mol% isopropylammonium chloride (iPAmHCl) to the precursor for the fabrication of the $FAPbI_3$ film, ensuring the specific effects of the $iPAmH^+$ cation. Similar to MACl, a substantial amount of the introduced iPAmHCl volatilized during the annealing process, with little iPAmHCl remaining at the $FAPbI_3$ grain boundaries, contributing to the stabilization of the α-phase and enabling the fabrication of PSCs with a certified PCE of 23.9%.

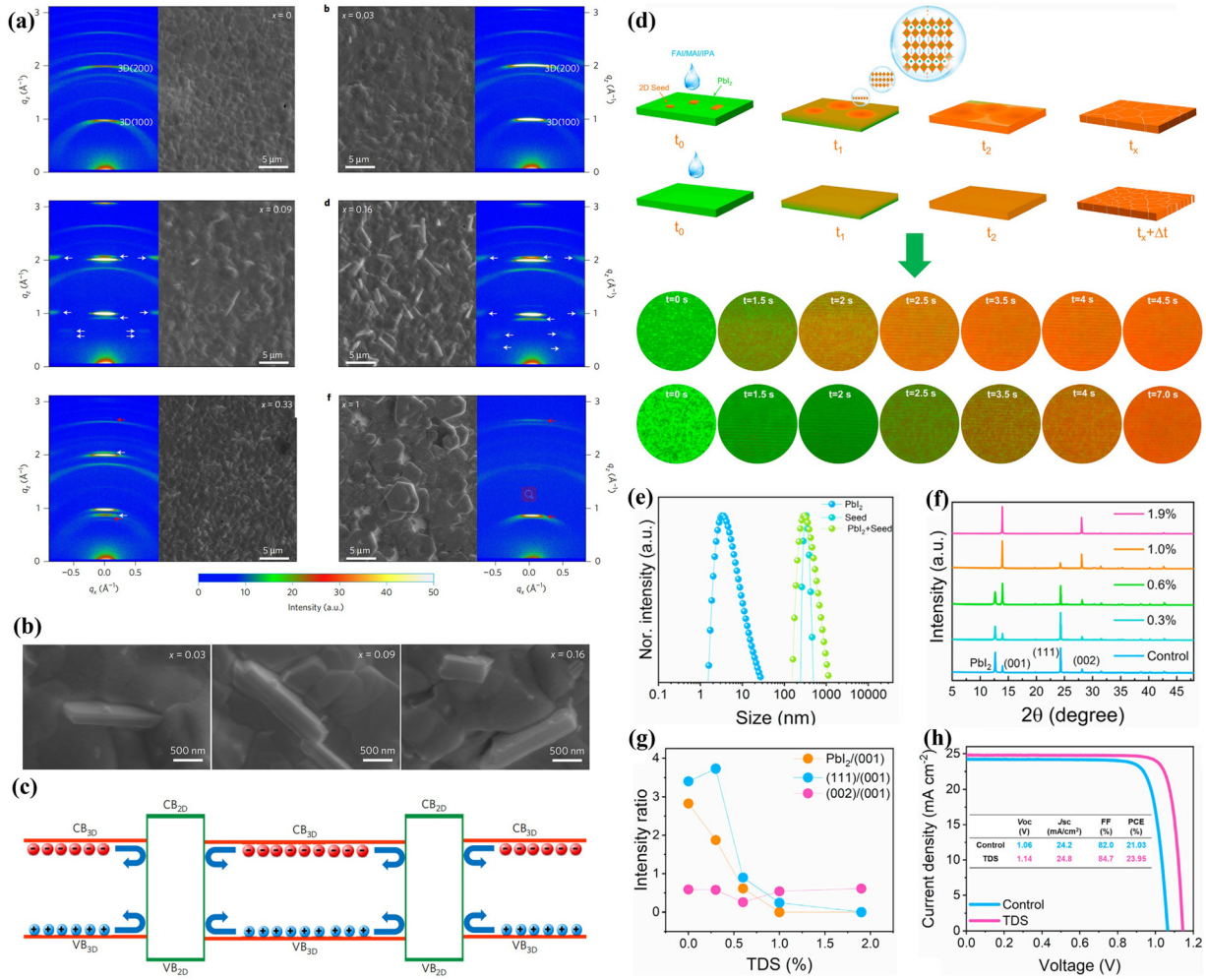

Fig. 7 (a) SEM images and 2D X-ray diffraction measurements of post-annealed perovskite films with different BA concentrations. (b) Enlarged SEM images of x = 0.03, 0.09 and 0.16 films. (c) Proposed electronic band offsets of the 2D/3D heterojunction. Reproduced with permission.[27] Copyright 2017, Springer Nature. (d) Schematic diagram of with/without BDA-seed-induced growth and the images of the PbI_2 film with/without 2D seed under a confocal laser scanning microscope at different reaction times after depositing organic salts. (e) Dynamic light scattering spectra of the solutions. XRD patterns (f) and different peak intensity ratios (g) of perovskite films with various seed concentrations. (h) *J*–*V* curves of control and BDA-modified PSCs. Reproduced with permission.[29] Copyright 2022, Elsevier.

The diammonium spacers with two ammonium groups can bond with a $[PbI_6]^{4-}$ octahedron on two sides, forming a DJ-type 2D perovskite. This structure provides favorable nucleation sites for the highly oriented growth of 3D perovskites.[49,50] In 2022, Zhao *et al.* introduced (BDA)PbI_4 (BDA = butane-1,4-diaminium) seed crystals into the PbI_2 precursor as nucleation centers for 2D/3D perovskite formation. The results revealed that the perovskite film bypassed the nucleation stage and directly entered the growth stage after being covered with organic salts.[29] The process of seed crystal-induced crystallization rapidly consumed the solute and significantly decreased the solution concentration. Consequently, it inhibited the random nucleation of the remaining 3D perovskite region without seeds, leading to the dominance of seed crystal-induced crystallization in the film formation process. It is noteworthy that the (BDA)PbI_4 itself inherently exhibited a high orientation of (00*L*). Therefore, the template-induced 3D perovskite demonstrated dominant and well-defined (001) and (002) peaks instead of the unfavorable (111) peaks. Eventually, the 2D phase transformed into grain boundaries after completing the orientation-induced growth, forming a type-I band alignment with 3D perovskite to passivate GB defects. This transformation resulted in a boost in PCE from 21.03% to 23.95% in mixed-dimensional PSCs (Fig. 7d-h). More reported organic spacer cations applied in bulk-incorporation type PSCs can be found in Table 1.

3.2. Surface treatment model

The surface passivation through the deposition of an organic spacer or a 2D perovskite layer is another crucial method to build 2D/3D heterojunctions in order to achieve both high efficiency and ultrastability in PSCs.[58] In general, defects on the surface of 3D perovskite, such as halide vacancies and undercoordinated Pb^{2+}, can be significantly passivated by introducing large spacer cations and their corresponding 2D perovskites. Simultaneously, the formation of 2D/3D heterojunctions through the surface passivation method rearranges the energy level structure at the interface between the 3D perovskite and the charge carrier transport layer, creating a staircase-like energy level structure that effectively enhances the carrier transport capacity. Additionally, the presence of large spacer cations at the interface can prevent water invasion and ion migration, thereby promoting excellent long-term stability of 2D/3D devices in various complex environments.

3.2.1. Aromatic spacers. In fact, aromatic compounds have long been used to construct 2D/3D heterojunctions using a surface deposition method.[59–61] In 2016, Docampo *et al.* reported 2D/3D perovskite by spin-coating a mixture solution of MAI:PEAI/IPA on the surface of 3D perovskite, and successfully observed (00l) diffraction peaks of $(PEA)_2(MA)_4Pb_5I_{16}$ by XRD measurement.[59] Two years later, Wang *et al.* developed a method by spin-coating PEAI solution on 3D perovskite and *in situ* formed a layered 2D PEA_2PbI_4.[62] Such a PEA_2PbI_4 2D perovskite capping layer induced Fermi-level splitting of the 2D/3D perovskite film under light illumination, leading to an enhanced V_{OC} and thus a PCE of 18.51% in 2D/3D PSCs. In 2022, Sun *et al.* reported *in situ* formed 2D perovskite by the deposition of a mixed solution of a hole transport material (HTM) (spiro-OMeTAD) and PEA spacers.[63] In this process, the high polar solvent like IPA was not used anymore, which reduced the damage to the 3D perovskite film, thus leading to a PCE of 21.09%.

In light of the unique properties of PEA spacers,[64,65] researchers have explored the molecular structure and extended the use of phenyl spacers such as benzylammonium (BnA),[66]

Table 1 An exhaustive list of recently reported organic spacer cations applied in bulk-incorporation type PSCs

Spacers	Device architecture	V_{OC} (V)	FF (%)	J_{SC} (mA cm^{-2})	PCE (%)	Ref.
PEA	ITO/SnO_2/$FA_{0.98}Cs_{0.02}PbI_3$/spiro-OMeTAD/Au	1.130	76.11	24.00	20.64	28
PABA	FTO/c-TiO_2/$MAPbI_3$/spiro-OMeTAD/Au	1.080	77.62	20.70	17.35	51
PhFA	ITO/SnO_2/$FA_{0.84}MA_{0.16}PbI_3$/spiro-OMeTAD/MoO_3/Ag	1.160	81.54	24.67	23.36	40
p-OHPhFA	ITO/SnO_2/$FA_{0.84}MA_{0.16}PbI_3$/spiro-OMeTAD/MoO_3/Ag	1.160	81.89	23.21	22.05	40
p-FPhFA	ITO/SnO_2/$FA_{0.84}MA_{0.16}PbI_3$/spiro-OMeTAD/MoO_3/Ag	1.160	81.73	23.24	22.03	40
MTIm	FTO/c-TiO_2/m-TiO_2/$[(MTIm)_2(Cs_{0.05}FA_{0.95})_{29}Pb_{30}I_{91}]_{0.85}$-$(MAPbBr_3)_{0.15}$/spiro-OMeTAD/Au	1.140	79.12	23.56	21.25	52
4-AEP	ITO/SnO_2/$MAPbI_3$/spiro-MeOTAD/Au	1.080	81.00	23.58	20.70	44
4AP	FTO/TiO_2/$FAPbI_3$/spiro-OMeTAD/Au	1.180	81.81	25.70	24.90	30
ThMA	ITO/SnO_2/$FA_{0.84}MA_{0.16}PbI_3$/spiro-OMeTAD/MoO_3/Ag	1.160	81.00	22.80	21.49	43
NpMA	ITO/SnO_2/$FA_{0.84}MA_{0.16}PbI_3$/spiro-OMeTAD/MoO_3/Ag	1.180	81.36	25.30	24.37	41
PEY	FTO/SnO_2/$(PEY_2PbI_4)_{0.02}MAPbI_3$/spiro-OMeTAD/Au	1.050	66.10	21.15	14.70	42
iPAm	—	1.159	79.80	25.79	23.85	48
BA	FTO/SnO_2/PCBM/$BA_{0.05}(FA_{0.83}Cs_{0.17})_{0.95}Pb(I_{0.8}Br_{0.2})_3$/spiro-OMeTAD/Au	1.140	80.00	22.70	20.60	27
TBA	ITO/PEDOT:PSS/$TBA_2MA_{19}Pb_{20}I_{61}$/PCBM/BCP/Ag	1.032	80.53	23.70	19.70	53
HEA	FTO/c-TiO_2/m-TiO_2/$(HEA)_2(Cs_{0.1}FA0.9)_{29}Pb_{30}I_{91}$/spiro-MeOTAD/Au	1.100	79.63	22.81	19.84	54
Gly	FTO/TiO_2/$CsPbI_2Br$(Gly-X)/spiro-OMeTAD/Au	1.330	80.92	16.04	17.26	55
GBA	PEN/ITO/PTAA/$FA_{0.7}MA_{0.25}Cs_{0.05}Pb(I_{0.93}Br_{0.07})_3$/PCBM/BCP/Ag	1.140	80.02	23.51	21.45	56
EDA	ITO/PEDOT:PSS/$FASnI_3$/PCBM/BCP/Ag	0.634	69.43	19.32	8.47	49
BDA	ITO/SnO_2/$FA_{0.75}MA_{0.25}PbI_3$/spiro-OMeTAD/Au	1.140	84.70	24.20	23.95	29
ODA	ITO/SnO_2/$Cs_{0.05}FA_{0.85}MA_{0.10}Pb(I_{0.97}Br_{0.03})_3$/spiro-OMeTAD/Ag	1.120	75.61	24.80	20.94	50
TETA	TO/SnO_2/$Cs_{0.05}FA_{0.85}MA_{0.10}Pb(I_{0.97}Br_{0.03})_3$/spiro-OMeTAD/Ag	1.100	74.03	25.22	20.57	50
EDBE	TO/SnO_2/$Cs_{0.05}FA_{0.85}MA_{0.10}Pb(I_{0.97}Br_{0.03})_3$/spiro-OMeTAD/Ag	1.150	76.66	25.88	22.68	50
TBA	ITO/PEDOT:PSS/$TBA_2MA_{19}Pb_{20}I_{61}$/PCBM/BCP/Ag	1.032	80.53	23.70	19.70	53
BiPi	FTO/TiO_2/$MAPbI_3$/spiro-OMeTAD/Au	1.100	77.00	23.51	20.03	57

phenylbutylammonium (PBA),[67] 4-fluorophen-ethylammonium (FPEA),[68,69] and pentafluorophenylethylammonium (FEA),[32] among others.[33,35,70–74] In 2019, Grätzel *et al.* employed FEA in highly efficient bilayer 2D/3D PSCs and successfully demonstrated the dominant generation of 2D perovskite on the surface of the 2D/3D bilayer through X-ray reflectivity (XRR) and grazing incidence X-ray diffraction (GIXRD) characterization. The $(FEA)_2PbI_4$ 2D perovskites exhibited approximately four layers in 2D/3D bilayers (about 8 nm) and displayed a larger angular distribution in the out-of-plane direction. Additionally, the perfluorinated 2D perovskite layer exhibited super hydrophobicity and inhibited ion motion, leading to comprehensive enhancement in moisture resistance and intrinsic stability of the obtained 2D/3D PSCs. In 2019, Sargent *et al.* creatively utilized 4-vinylbenzylammonium (VBA) to create well-ordered perovskite quantum wells (PQWs) (also known as low dimensional perovskites) on top of 3D perovskite layers.[33] As shown in Fig. 8a–d, VBA featured an additional terminal vinyl group on the *para* position of the ammonium group in the benzene ring. The adjacent vinyl groups formed an extended conjugate

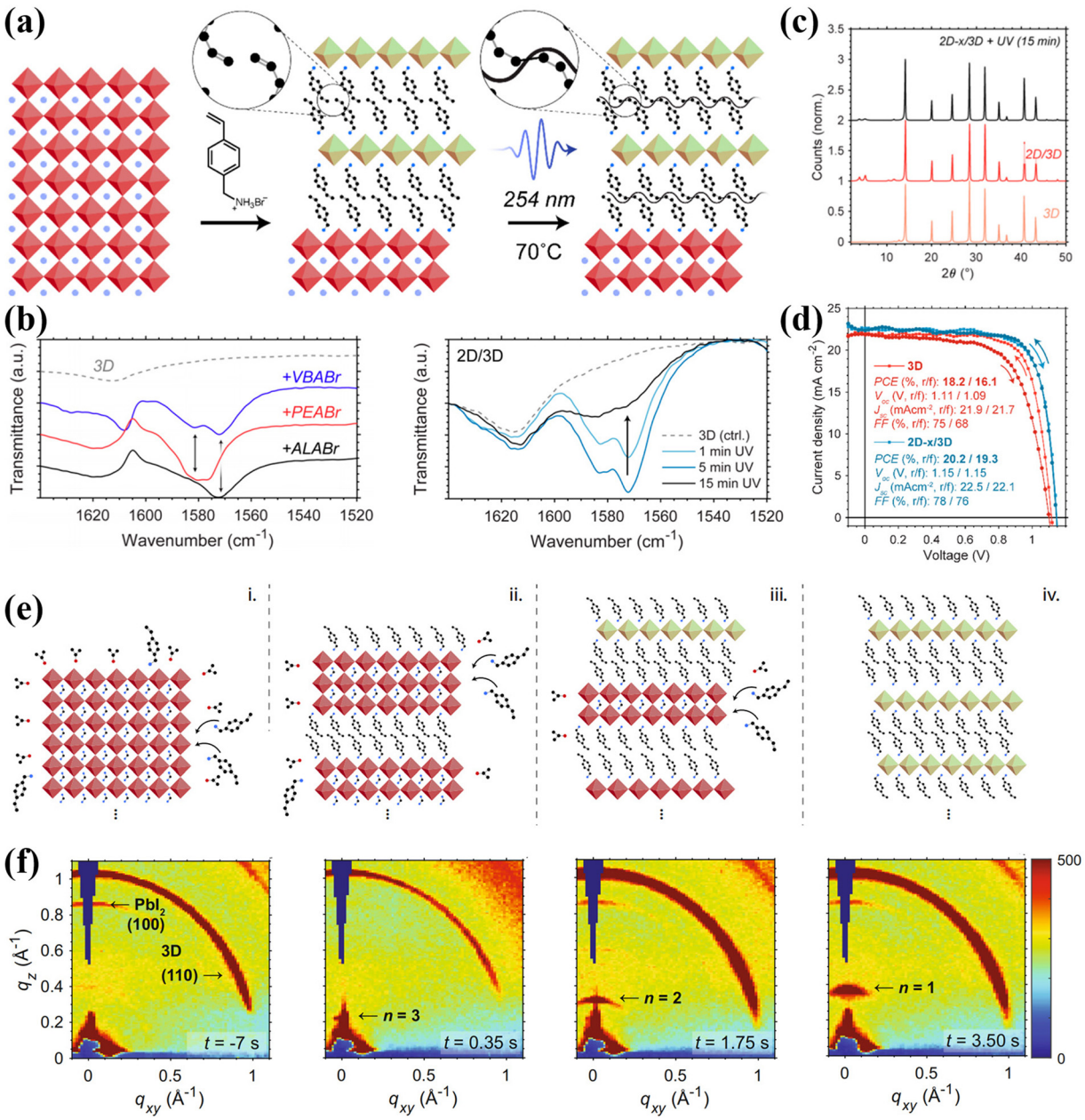

Fig. 8 (a) Schematic illustrating the process by which formation of cross-linked 2D perovskites atop a 3D layer is achieved using VBABr. (b) Fourier transform infrared spectra of films treated with VBABr, PEABr, and ALABr and the 2D/3D VBABr-treated films with different durations of UV light (254 nm) exposure. (c) XRD patterns for the 3D film and the 2D/3D film with/without UV exposure. (d) *J*–*V* curves of VBA-based 2D/3D perovskites. Reproduced with permission.[33] Copyright 2019, American Chemical Society. (e) Proposed 3D-to-2D conversion mechanism by VBA spacers. (f) *In situ* GIWAXS patterns for VBA-treated films. Reproduced with permission.[35] Copyright 2021, Springer Nature.

system undergoing photochemical cross-linking under UV photoexcitation (~250 nm) to produce new covalent bonds when forming 2D perovskites.[75,76] These cross-linked VBA-based 2D/3D perovskite films exhibited improved crystallinity, resulting in enhanced V_{OC}, negligible hysteresis, and increased hydrophobic properties compared to uncross-linked counterparts such as PEA-based and allylammonium (ALA)-based heterojunctions. To gain further insight into the formation mechanism of VBA-based 2D/3D heterojunction films, *in situ* GIWAX measurements were conducted to gather information regarding the orientation and *d*-spacing of diffractive species before, during, and after the exposure of 3D perovskites to VBA spacers.[35] For the $(MAPbBr_3)_{0.05}$-$(FAPbI_3)_{0.95}$ perovskite, upon exposure to VBA spacers, 2D perovskite with n = 3 initially formed and its dimension gradually decreased in subsequent stages, undergoing a progressive dimensional reduction from 3D fragments to $n = 3 \rightarrow 2 \rightarrow 1$ (Fig. 8e and f).

Thiophenyl aromatic compounds are also important organic spacers for the construction of 2D/3D heterojunctions on the surface of 3D perovskite.[36,77] As mentioned above, 2D/3D heterojunctions can regulate the arrangement of energy levels to enhance charge extraction. To investigate this mechanism more thoroughly, Grancini *et al.* developed an innovative technique called ultraviolet photoemission spectroscopy (UPS) depth profiling. This technique allowed them to probe the energetic landscape within the bulk of materials and across buried interfaces, accurately measuring the progression of the vacuum level and valence band positions as a function of film depth. They further utilized this technique to provide an *in situ* measurement of the interfacial energy level alignment in a 2D/3D system constructed using ThMAX (X = Cl, Br, or I) (Fig. 9a).[78] The valence bands of 2D perovskites composed of ThMAI and ThMABr bent downward, resulting in an energy level alignment that promoted hole extraction. On the other hand, the valence bands of 2D perovskites composed of ThMACl showed an upward slope, creating a certain energy barrier for hole transport. Importantly, the 2D perovskites based on ThMAI and ThMABr exhibited a clear transition from n-type to p-type materials compared to the 3D perovskite. This transition led to the formation of a p–n junction at the interface between the 3D and 2D perovskites, significantly enhancing charge extraction and reducing interface recombination (Fig. 9b and c). Additionally, Grancini and colleagues also investigated the inhibitory effects of thiophenyl-based 2D perovskites on ion migration.[79] Pure 2D perovskites based on ThMAI and 3-thiophenemethylammonium iodide (3-TMAI) can embed small MA cations that migrate from the 3D bulk underneath and immobilize them to form a new quasi-2D structure. In this transition process, the MA cations were consumed. On the other hand, 2D perovskites based on 2-thiopheneethylammonium iodide (2-TEAI) physically blocked the MA cations at the 2D/3D interface, inhibiting ion migration and preserving the purity of the 2D phase. Therefore, although different thiophenyl-based 2D perovskites employed different mechanisms to block ion migration, 2D/3D hybrid devices fabricated by using ThMAI, 3-TMAI and 2-TEAI all exhibited improved long-term stability compared to the pristine device.

Imidazole (IZ) is a unique diammonium molecule with an aromatic structure that can form additional hydrogen bonding with a $[PbI_6]^{4-}$ framework. Due to its delocalized π bonding, it may exhibit low reactivity with its surroundings, leading to additional electrical conductivity.[82,83] However, IZ has an unfavorable ionic radius of 258 pm, which is close to the upper limit of the tolerance factor. Therefore, it is not considered a suitable spacer for 2D perovskite fabrication.[82] In 2022, Tu *et al.* successfully demonstrated the formation of 2D/3D heterojunctions through post-treatment with imidazole hydrobromide (IZBr) and achieved an outstanding PCE of 23.25% for MA-free ($FA_{0.9}Cs_{0.1}PbI_3$) PSCs.[84] Other imidazolium-based cations such as benzimidazolium (BIZ) and benzodiimidazolium (Bdi) spacers have larger ionic radii and stronger π conjugation effects, making them more suitable for 2D/3D heterojunction fabrication.[85] In 2021, Feng *et al.* reported the facile *in situ* formation of a layered 2D $(BIZ)_2PbI_3Br$ perovskite by incorporating benzimidazolium iodine (BIZI) on a 3D $CsPbI_2Br$ absorber. The resulting 2D $(BIZ)_2PbI_3Br$ exhibited remarkable defect passivation and moisture resistance for the 3D perovskite, leading to improved photovoltaic performance in an inverted (p–i–n) PSC.[86] More recently, based on benzimidazole, Chen *et al.* designed highly conjugated fluorinated benzimidazolium halides (FBImX, X = I or Br) as passivators for 2D/3D perovskite. By introducing double fluoride atoms in the *meta*-position of the imidazole group, fluoride effectively enhanced the hydrophobicity of the film and passivated both anion and cation vacancies present in 3D perovskite.[80] As a result, the best PCE of 23.00% was achieved for FBImBr-incorporated PSCs, along with a high V_{OC} of 1.17 V and an FF of 81.80%. The FBImBr-modified device exhibited excellent operational stability, maintaining 86% of the initial PCE after 1300 h under 25% relative humidity (Fig. 9d–f).

Generally, fullerene (C_{60})[87] and its derivatives, such as phenyl-C_{61}-butyric acid methyl ester (PCBM),[88] C_{60}-substituted benzoic acid self-assembled monolayer (C_{60}-SAM)[89] and [6,6]-phenyl-C_{61}-butyric acid-dioctyl-3,3'-(5-hydroxy-1,3-phenylene)-bis(2-cyanoacrylate) ester (PCBB-2CN-2C8),[90] are used as electron transport materials due to their high electron affinity and strong electron acceptance ability. However, the larger molecular size of C_{60} (with a van der Waals diameter of ~7 Å) compared to the $[PbI_6]^{4-}$ octahedron (with a size of 6.3 Å) makes it difficult for C_{60} to fit into the $[PbI_6]^{4-}$ octahedron layer to form a 2D structure.[81] To overcome this barrier, Yang *et al.* synthesized a novel amino-functionalized fullerene derivative called C_{60}-BPAM, in which two amino groups were grafted onto C_{60} using a pyrrolidine–phenyl linker. They then fabricated a DJ-type (C_{60}-BPAM)PbI_4 2D perovskite on top of a 3D $MAPbI_3$ perovskite by drop-casting an anti-solvent to form a 2D/3D heterojunction.[81] As a result, C_{60}-BPAM significantly facilitated electron transport and improved the humidity stability of the 2D perovskite structure due to the highly conductive and hydrophobic C_{60} tail. This strategy presents a promising new approach for the preparation of 2D/3D heterojunctions (Fig. 9g and h).

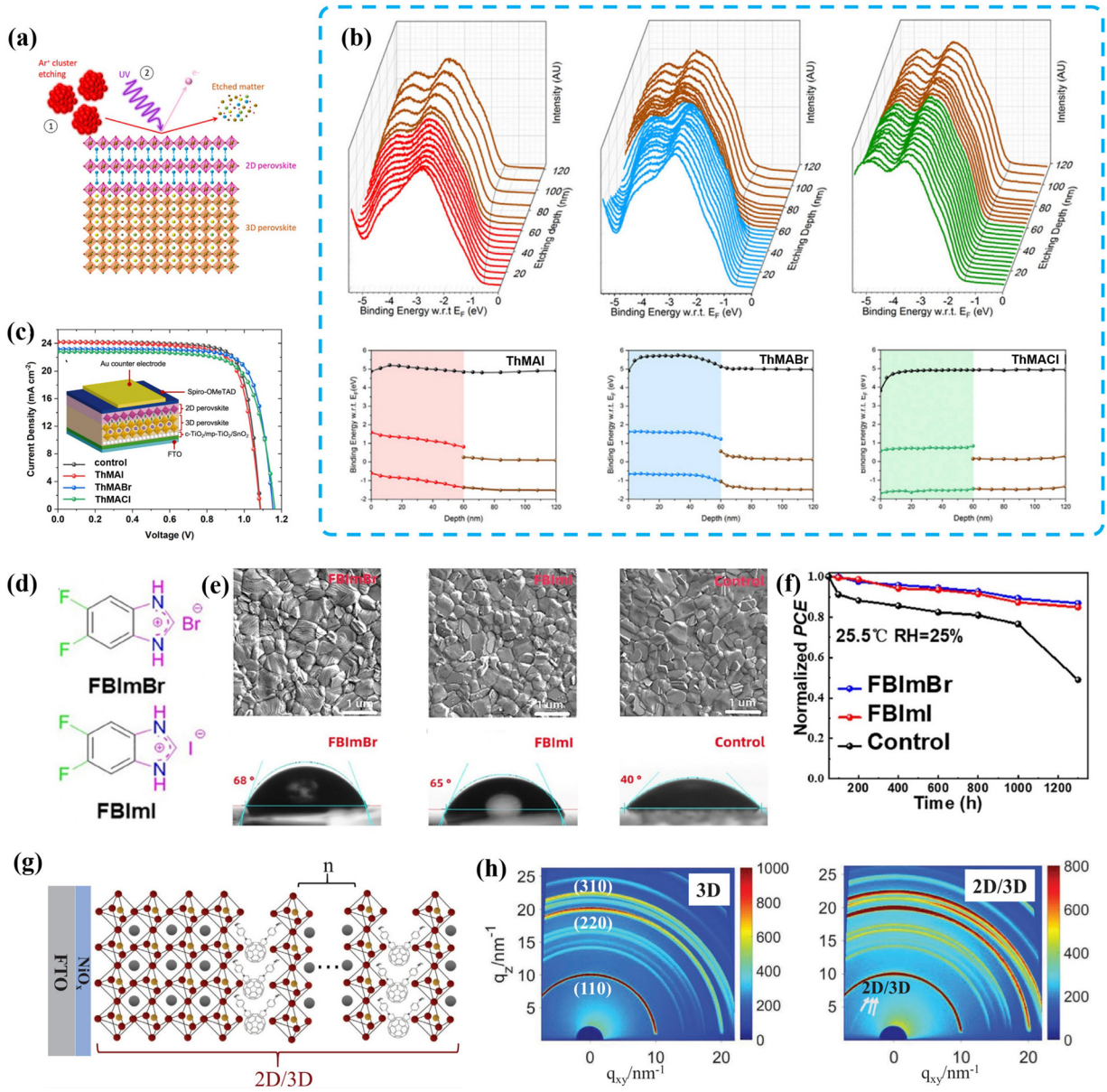

Fig. 9 (a) Schematic representation of the UPS depth profiling technique. (b) Measured UPS spectra and the corresponding energetic level diagrams of ThMAI, ThMABr, and ThMACl with the 3D perovskite layer. (c) *J*–*V* curves of the champion cells of 3D and 2D/3D PSCs employing ThMAI, ThMABr, and ThMACl. Reproduced with permission.[78] Copyright 2021, Elsevier. (d) Chemical structures of FBImBr and FBIml. (e) SEM images and water contact angle images of FBImBr, FBIml and control perovskite films. (f) Environmental stability for the FBImBr, FBIml and control devices. Reproduced with permission.[80] Copyright 2023, Springer Nature. (g) Schematic illustration of the structure of Dion–Jacobson phase 2D/3D (C_{60}-BPAM). (h) 2D-GIXRD profiles of 3D and 2D/3D perovskite films. Reproduced with permission.[81] Copyright 2022, John Wiley & Sons, Inc.

3.2.2. Aliphatic spacers. Despite aliphatic spacers are considered to be weaker than aromatic spacers in terms of charge transport, their longer carbon tails endow them with higher structural degrees of freedom and hydrophobic properties, thereby enabling a wide range of applications.[91] In 2018, Huang *et al.* utilized short-chain aliphatic BA and the corresponding iodide (BAI) as passivating agents to investigate 2D/3D stacking structures.[92] They found that BA promoted the formation of a pure 2D BA_2PbI_4 perovskite by reacting with $MAPbI_3$. The pure BA_2PbI_4 exhibited more organic spacers than the mixture of 2D perovskites, indicating superior protective effects. On the other hand, the reaction between BAI and $MAPbI_3$ resulted in inferior $(BA)_2(MA)_{n-1}Pb_nI_{3n+1}$ with various *n* values, leading to a rougher 2D perovskite layer compared to the BA-constructed 2D perovskite (Fig. 10a and b). In 2021, Noh *et al.* developed another method called the solid-state in-plane growth (SIG) process, which involved integrating a pre-formed 2D BA_2PbI_4 perovskite capping layer onto 3D perovskite surfaces through mechanical and thermal pressure.[34] The SIG process allowed for controlled deposition of a pure and highly crystalline 2D $(BA)_2PbI_4$ perovskite layer on top of a 3D perovskite layer without the presence of any quasi-2D phases. As a result, the intact 2D/3D

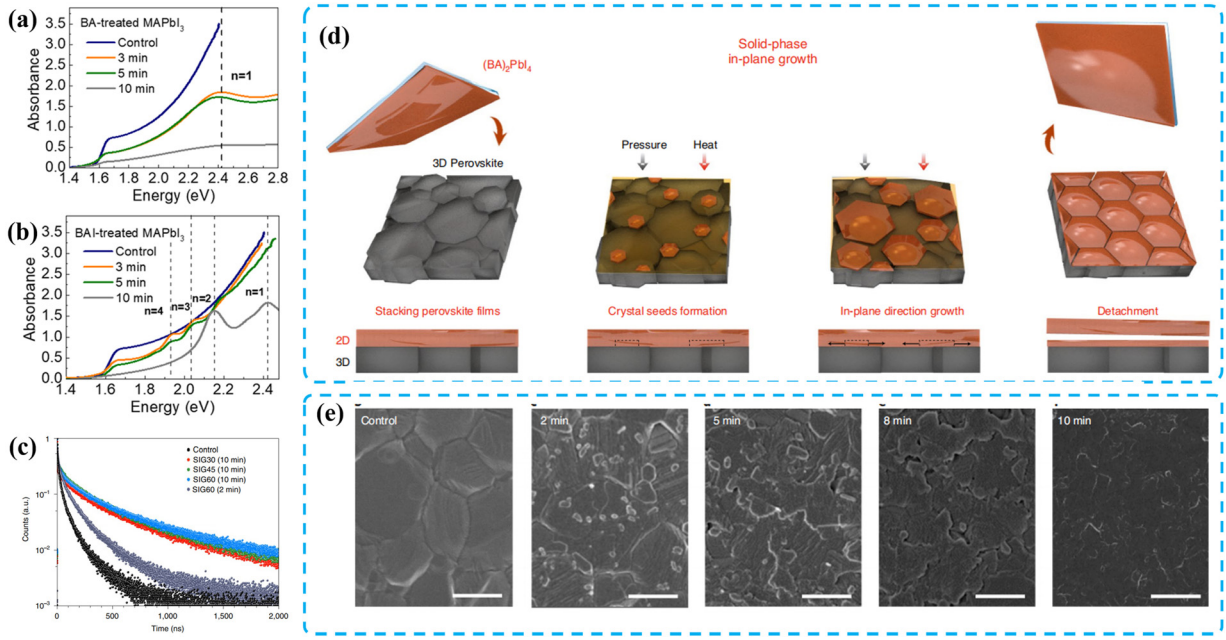

Fig. 10 Absorption spectra of (a) BA-treated $MAPbI_3$ films and (b) BAI-treated $MAPbI_3$ films with different reaction times. Reproduced with permission.[92] Copyright 2018, American Chemical Society. (c) Time-resolved photoluminescence decay curves of the control and SIG-processed 2D/3D films. (d) Top-view and cross-sectional sketches of the manufacturing of a $(BA)_2PbI_4$ film on a 3D perovskite substrate *via* the SIG method. (e) The 2D/3D perovskite film fabricated under SIG60 conditions after 2 min, 5 min, 8 min and 10 min processing times. Reproduced with permission.[34] Copyright 2021, Springer Nature.

heterojunction enhanced the carrier lifetime and facilitated the design of the local electric field distribution at the junction, leading to a significant improvement in the V_{OC} of PSCs (Fig. 10c–e). Recently, Mohite *et al.* explored the use of acetonitrile (MeCN) as a solvent to dissolve 2D perovskites ($BA_2MA_{n-1}Pb_nI_{3n+1}$, n = 1 to 4) without destroying the underlying 3D perovskite.[93] MeCN was found to possess an appropriate dielectric constant and Gutmann donor number. With an increase in the n value of the 2D perovskite, a transition from type I heterojunction to type II heterojunction was observed due to changes in energy level alignment. Among them, the type II heterojunction achieved with $BA_2MA_2Pb_3I_{10}$ (n = 3) and the 3D perovskite exhibited near-perfect alignment of the valence band edges for 3D and 2D perovskites. This alignment was considered ideal for hole extraction and created a significant energy barrier for electron transport. Consequently, the fabricated 2D/3D PSC incorporating a pure n = 3 2D component achieved a champion PCE of 24.5% with an impressive V_{OC} of 1.20 V.

The long-chain in aliphatic organic spacers can provide the possibility of forming more reaction sites, which can strengthen the interaction between the spacers and inorganic $[PbI_6]^{4-}$ framework, thereby improving the film's photophysical properties and device performance.[91,94] In 2021, Lan *et al.* utilized a viscous polymer named polypropylene glycol bis (2-aminopropyl ether) (A-PPG) with a number-average molecular weight (Mn) of 400 to create a quasi-2D layer on the surface of 3D perovskite *in situ*. A-PPG had the ability to partially dissolve excess PbI_2 and perovskite, and it was applied in a one step spin-coating process with the addition of chlorobenzene as the anti-solvent in advance.[95] Moreover, unlike other spacer cations, the lone electron pairs of the ether-oxygen in A-PPG can also form coordination bonds with undercoordinated Pb^{2+}, significantly contributing to defect passivation and reducing non-radiative recombination. Consequently, the A-PPG-modified 2D/3D PSC exhibited an optimized PCE of 22.24% with a distinguished V_{OC} of 1.21 V. The device also maintained 90% of its original PCE in an ambient atmosphere after 50 days, demonstrating extraordinary humidity stability. More reported organic spacers applied in surface-treatment type PSCs are summarized in Table 2.

3.3. Bulk incorporation and surface treatment coexisting model

In view of the advantages of 2D/3D perovskite heterojunctions in modifying grain boundaries and passivating surface defects, researchers have started exploring the combination of these two methods to create a coexisting type 2D/3D heterojunctions. Specifically, the process involves adding spacers to the perovskite precursor, resulting in a 2D/3D heterojunction within the bulk of the deposited 3D perovskite film. Subsequently, a solution containing spacers (or 2D perovskites) is dropped onto the film surface after annealing, creating a capping 2D perovskite layer after post-treatment. Furthermore, there exist many other approaches for constructing the same structure, which we will discuss in the following discussion and mainly focus on aromatic and aliphatic organic spacers.

3.3.1. Aromatic spacers. Lan *et al.* designed a pyridinyl organic ammonium salt named 2-(2-pyridyl)ethylamine iodide (2-PyEAI) and applied the above method to prepare a 2D/3D

Table 2 An exhaustive list of recently reported organic spacer cations applied in surface-treatment type PSCs

Spacers	Device architecture	V_{OC} (V)	FF (%)	J_{SC} (mA cm^{-2})	PCE (%)	Ref.
BnA	FTO/c-TiO_2/m-TiO_2/SnO_2/3D perovskite/BnA-based 2D perovskite/spiro-OMeTAD/Au	1.078	78.80	24.48	20.79	66
PEA	FTO/TiO_2/$Cs_{0.05}(MA_{0.12}FA_{0.88})_{0.95}Pb(I_{0.88}Br_{0.12})_3$/$PEA_2PbI_4$/PEAI-spiro-OMeTAD/Au	1.170	79.00	22.93	21.09	63
PBA	ITO/NiO_X/$(Cs_{0.07}FA_{0.95}PbI_{2.95})_{0.85}(MAPbBr_3)_{0.15}$/PBA-based 2D perovskite/PCBM:C_{60}/Zr(acac)$_4$/Au	1.170	83.92	22.16	21.76	67
FPEA	FTO/c-TiO_2/m-TiO_2/$Cs_{0.1}(FA_{0.83}MA_{0.17})_{0.9}Pb(I_{0.83}Br_{0.17})_3$/$FPEA_2PbI_4$/spiro-OMeTAD/Au	1.126	80.00	22.80	20.54	69
FEA	FTO/c-TiO_2/m-TiO_2/$FA_{0.92}MA_{0.04}Cs_{0.04}PbI_3$/FEA-based 2D perovskite/spiro-OMeTAD/Au	1.096	78.40	25.79	22.16	32
3Cl-BA	FTO/c-TiO_2/m-TiO_2/$MAPbI_3$/$(3Cl\text{-}BA)_2PbI_4$/carbon	0.980	63.00	21.31	13.22	73
CF3PMA	ITO/PTAA/$MAPbI_3$/CF_3PMA-based 2D perovskite/PCBM/BCP/Ag	1.070	72.22	19.38	15.01	71
CF3PEA	FTO/TiO_2/$FA_{0.85}MA_{0.15}PbI_3$/$(CF_3PEA)_2FAPb_2I_7$/spiro-OMeTAD/Au	1.130	80.78	25.29	23.10	72
PTA	FTO/c-TiO_2/SnO_2/$MAPbI_3$/PTA-based 2D perovskite/spiro-MeOTAD/Ag	1.104	81.90	23.39	21.26	96
OHPEA	ITO/SnO_2/$Rb_{0.05}Cs_{0.05}[(FA_{0.83}MA_{0.17})]_{0.9}Pb(I_{0.83}Br_{0.17})_3$/OHPEA-based 2D perovskite/spiro-MeOTAD/Ag	1.220	75.50	23.25	21.38	97
ABA	FTO/NiO_X/$MAPbI_3$/PCBM/Rhodamine 101/Ag	1.105	81.90	23.42	21.18	70
VBA	ITO/TiO_2/$(MAPbBr_3)_{0.15}(FAPbI_3)_{0.85}$/VBA-based 2D perovskite/spiro-OMeTAD/Au	1.150	78.00	22.50	20.20	33
TFPhFA	FTO/SnO_2/$FA_{0.93}MA_{0.07}PbI_3$/spiro-MeOTAD/Au	1.160	81.26	25.42	24.00	98
PDA	FTO/TiO_2/$(Cs_{0.05}(FA_{0.83}MA_{0.17})_{0.95}Pb(I_{0.83}Br_{0.17})_3$/PDA-based 2D perovskite/spiro-MeOTAD/Ag	1.145	77.89	23.78	21.15	74
XDA	FTO/c-TiO_2/SnO_2/$MAPbI_3$/XDA-based 2D perovskite/spiro-MeOTAD/Ag	1.134	76.92	23.78	20.74	99
IZ	ITO/SnO_2/$FA_{0.9}Cs_{0.1}PbI_3$/IZ-based 2D perovskite/spiro-MeOTAD/Ag	1.172	80.76	24.57	23.25	84
BIZ	ITO/NiO_X/$CsPbI_2Br$/$(BIZ)_2PbI_3Br$/PCBM/Ag	1.151	79.79	15.59	14.32	86
FBIm	ITO/SnO_2/$FAPbI_3$/$(FBIm)_2PbBr_4$/spiro-MeOTAD/MoO_3/Ag	1.170	81.80	24.03	23.00	80
ThMA	FTO/c-TiO_2/m-TiO_2/SnO_2/$[(FAPbI_3)_{0.87}(MAPbBr_3)_{0.13}]_{0.92}(CsPbI_3)_{0.08}$/ThMA-based 2D perovskite/spiro-OMeTAD/Au	1.150	78.00	23.20	20.80	78
3-TMA	FTO/c-TiO_2/m-TiO_2/SnO_2/$MAPbI_3$/quasi-2D 3-TMA perovskite/spiro-MeOTAD/Au	1.132	77.10	23.60	20.59	79
2-TEA	FTO/c-TiO_2/m-TiO_2/SnO_2/$MAPbI_3$/$(2\text{-}TEA)_2PbI_4$/spiro-MeOTAD/Au	1.117	73.70	23.60	19.42	79
OA	FTO/SnO_2/$(FAPbI_3)_{0.95}(MAPbBr_3)_{0.05}$/OA-based 2D perovskite/PTAA/Au	1.180	80.80	24.70	23.60	100
1,8-ND	ITO/SnO_2/$FA_{0.92}MA_{0.08}PbI_3$/spiro-OMeTAD/Au	1.150	83.00	24.90	23.80	101
C_{60}-BPAM	FTO/NiO_X/$MAPbI_3$/(C_{60}-BPAM)PbI_4/PCBM/BCP/Ag	1.090	78.53	23.61	20.21	81
CA	ITO/PEDOT:PSS/$MAPbI_3$/PCBM/Rhodamine 101/LiF/Ag	0.920	77.26	19.29	13.86	60
BA	FTO/SnO_2/$(FAPbI_3)_{0.95}(MAPbBr_3)_{0.05}$/$BA_2PbI_4$/spiro-OMeTAD/Au	1.185	83.90	24.70	24.59	34
HA	FTO/SnO_2/$(FAPbI_3)_{0.80}(CsPbI_3)_{0.07}(MAPbBr_3)_{0.13}$/HA-based 2D perovskite/spiro-OMeTAD/Ag	1.140	76.00	23.76	20.62	102
HTA	ITO/SnO_2/$(FAPbI_3)_{0.95}(MAPbBr_3)_{0.05}$/HTA-based 2D perovskite/spiro-OMeTAD/Ag	1.170	79.55	22.69	21.12	103
4-ABA	FTO/SnO_2/$Cs_{0.05}(FA_{0.83}MA_{0.17})_{0.95}Pb(I_{0.83}Br_{0.17})_3$/4-ABA-based 2D perovskite/spiro-OMeTAD/Au	1.200	78.55	24.57	23.16	104
AVA	FTO/c-TiO_2/m-TiO_2/$MAPbI_3$/AVA-based 2D perovskite/spiro-MeOTAD/Au	1.060	76.00	22.30	18.00	105
A43	FTO/c-TiO_2/m-TiO_2/$MA_{0.9}FA_{0.1}PbI_3$/$(A43)_2PbI_4$/spiro-MeOTAD/Au	1.110	79.30	22.87	20.12	106
A-PPG	FTO/TiO_2/$(FAPbI_3)_{0.84}(CsPbI_3)_{0.06}(MAPbBr_3)_{0.10}$/A-PPG-based 2D perovskite/spiro-OMeTAD/Au	1.210	78.97	23.27	22.24	95
DMEDA	ITO/SnO_2/$MAPbI_3$/DMEDA-based 2D perovskite/spiro-OMeTAD/Ag	1.140	78.00	22.57	20.18	107
DETA	ITO/NiO_X/$Cs_{0.05}(FA_{0.85}MA_{0.15})_{0.95}Pb(I_{0.85}Br_{0.15})_3$/DETA-based 2D perovskite/PCBM/BCP/Ag	1.100	83.33	21.73	19.94	94
TETA	ITO/NiO_X/$Cs_{0.05}(FA_{0.85}MA_{0.15})_{0.95}Pb(I_{0.85}Br_{0.15})_3$/TETA-based 2D perovskite/PCBM/BCP/Ag	1.110	83.90	21.61	20.13	94
TEPA	ITO/NiO_X/$Cs_{0.05}(FA_{0.85}MA_{0.15})_{0.95}Pb(I_{0.85}Br_{0.15})_3$/TEPA-based 2D perovskite/PCBM/BCP/Ag	1.120	84.81	22.39	21.28	94
PEHA	ITO/NiO_X/$Cs_{0.05}(FA_{0.85}MA_{0.15})_{0.95}Pb(I_{0.85}Br_{0.15})_3$/PEHA-based 2D perovskite/PCBM/BCP/Ag	1.130	84.90	22.63	21.79	94
EDA	ITO/NiO_X/PTAA/$Cs_{0.05}(FA_{0.95}MA_{0.05})_{0.95}Pb(I_{0.95}Br_{0.05})_3$/EDA-based 2D perovskite/PCBM/BCP/Ag	1.200	81.90	25.20	24.70	108
ODA	FTO/c-TiO_2/m-TiO_2/$(FA_{0.85}MA_{0.15})Pb(I_{0.85}Br_{0.15})_3$/(ODA)$PbI_4$/spiro-MeOTAD/Au	1.100	81.00	24.20	21.60	109
EDBE	ITO/SnO_2/$Cs_{0.2}FA_{0.8}Pb(I_{0.7}Br_{0.3})_3$/EDBE-based 2D perovskite/spiro-OMeTAD/Ag	1.280	78.50	18.85	18.85	110

hybrid PSC with a high efficiency of 23.2%.[111] Meanwhile, Liu *et al.* made groundbreaking advancements by developing 2-thiopheneformamidinium bromide (ThFABr) to passivate the inevitable defects present in both the bulk and surface of perovskite films, achieving an ultralong carrier lifetime exceeding 20 μs and carrier diffusion lengths longer than 6.5 μm (Fig. 11a and b).[112] Typically, the carrier lifetime and diffusion length are closely related to the density of defects. As shown in Fig. 11c, the PL intensity enhanced more pronouncedly in the coexisting type 2D/3D PSC as the excitation fluence increased, indicating that the trap states were filled more rapidly during the excitation process, confirming the effective passivation of defects. Importantly, the passivation of defects was facilitated by the incorporation of ThFABr, resulting in the formation of 2D perovskites in the bulk and on the surface of 3D perovskites (Fig. 11d–f). Moreover, the thickness of perovskite films was generally less than 1 μm due to the limited carrier diffusion length. The ultra-long carrier lifetime and diffusion lengths made it possible to fabricate film thickness-insensitive devices for their future commercialization. Consequently, the coexisting type 2D/3D PSCs achieved a champion PCE of 24.69% (film thickness < 1 μm) and an excellent PCE of 24.15% (film thickness > 1.1 μm (Fig. 11g and h).

On the other hand, in 2021, He *et al.* reported a heterogeneous 2D/3D tin-halide PSC ($FASnI_3$) through the substitution of FAI with FPEABr. They demonstrated that 2D components can be transferred from the bulk phase to the surface of the 3D perovskite during the grain growth process.[115] It was observed that, on one hand, there was an extensive oxidation process from Sn^{2+} to Sn^{4+} during the aging of $FASnI_3$. The authors proved that the introduction of FPEABr, which formed a 2D phase, prevents the oxidation of Sn^{2+} to Sn^{4+}. On the other hand, the 2D tin-perovskite layer based on $FPEA^+$ blocked the water penetration due to the presence of bonded F atoms, resulting in significantly improved humidity stability. Consequently, the highly oriented and stable 2D/3D PSC achieved an outstanding PCE of 14.81%, with a certified PCE of 14.03%, setting a new record for $FASnI_3$-based PSC at that time.

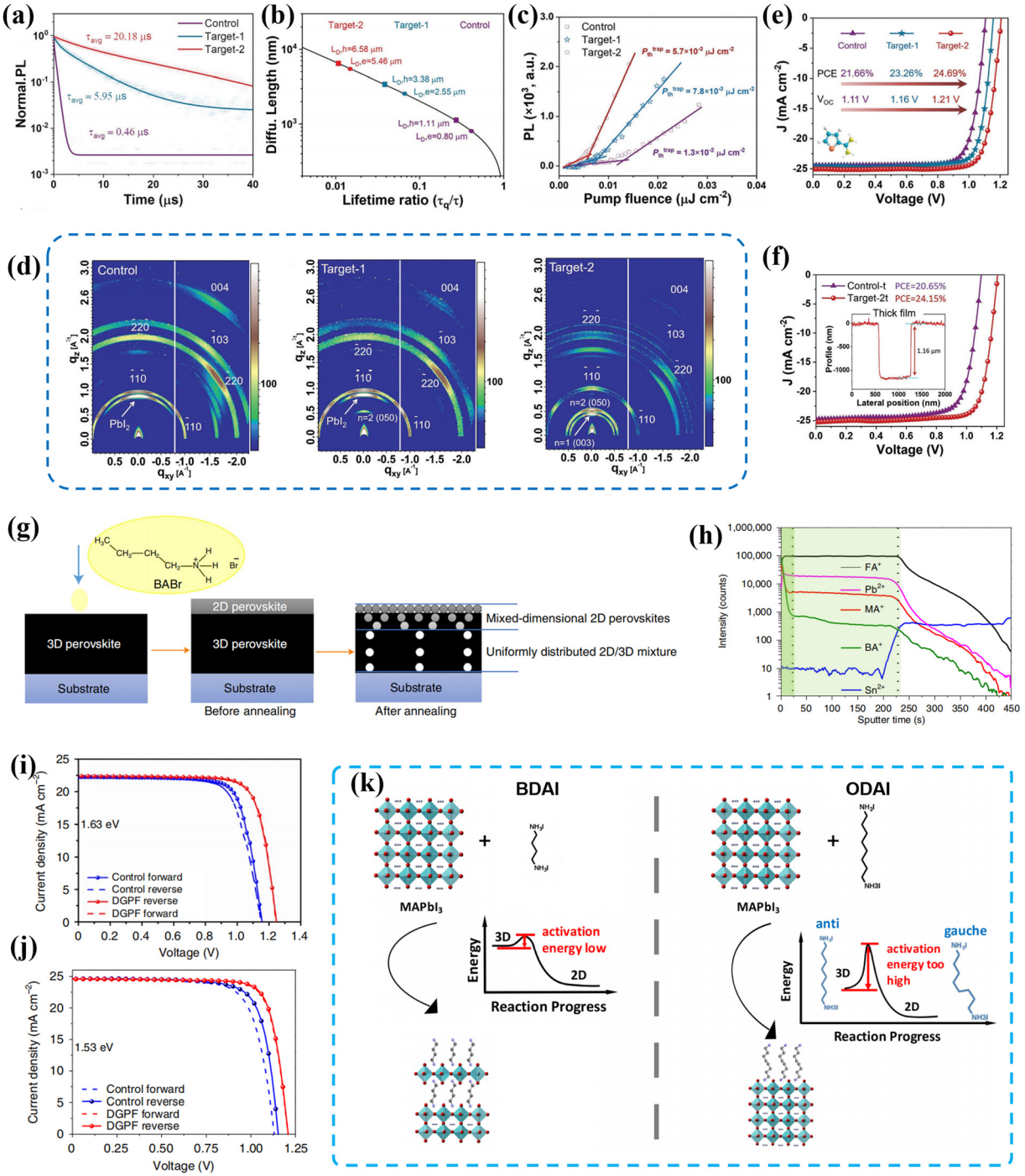

Fig. 11 (a) TRPL decay spectra, (b) the diffusion length of holes and electrons, (c) pump fluence dependent PL intensity and (d) GIWAX measurements for the control, bulk incorporation type (target-1) and coexisting type (target-2) 2D/3D films using ThFABr. *J*–*V* curves of PSCs based on (e) control, target-1 and target-2 perovskites and (f) a thick perovskite film. Reproduced with permission.[112] Copyright 2023, John Wiley & Sons, Inc. (g) Schematic diagram of the DGPF film. (h) ToF-SIMS depth profile of the DGPF perovskite film deposited on an ITO substrate. *J*–*V* curves based on the 1.63 eV(i) and 1.53 eV(j) perovskite. Reproduced with permission.[113] Copyright 2021, Springer Nature. (k) Schematic demonstration of why BDA treatment can induce respective 2D hybrid perovskite formation, while ODA stays only at the surface or grain boundaries without affecting bulk properties. Reproduced with permission.[114] Copyright 2016, American Chemical Society.

3.3.2. Aliphatic spacers. For aliphatic spacer cations, in 2021, Li *et al.* designed a dimensionally graded perovskite formation (DGPF) approach to achieve a homogeneously distributed self-passivated 2D/3D perovskite structure in the bulk. This structure was further capped by a stepped mixed-dimensional 2D perovskite with a wider-band gap through thermal annealing of the 3D perovskite layer covered with a spin-coated *n*-butylammonium bromide (BABr) solution.[113]

The introduction of the BA moiety immensely passivated anti-site defects like Pb_{Br} and Pb_I, which were known as deep-level defects that can cause carrier recombination. Using the DGPF technique, the 2D/3D hybrid PSC demonstrated a maximum hysteresis-free PCE of 21.54% with a band gap-voltage offset (W_{OC}) of 0.39 V in a 1.63 eV perovskite system (RbCsMAFA-based) and a champion PCE of 23.78% with a low W_{OC} of 0.326 V in an approximately 1.53 eV perovskite system ($Cs_{0.03}(FA_{0.97}MA_{0.03})_{0.97}Pb(I_{0.97}Br_{0.03})_3$) (Fig. 11g–j). However, not all organic spacers can be applied to generate 2D perovskites within the 3D perovskite bulk through post-treatment. Jen *et al.* found that the introduction of BDA with a short carbon chain (the same number of carbon atoms as BA) could promote the transformation from 3D perovskite to 2D perovskite during post-treatment, whereas the octane-1,8-diaminium (ODA) (with twice the number of carbon atoms compared to BA and BDA) could only insert into the grain boundaries within the 3D perovskite bulk without any dimension transformation.[114] The fast dimension transformation caused by BDA could be attributed to the high thermodynamic stability of 2D perovskites and the low activation energy of the transformation process. In contrast, the failure of ODA to facilitate dimensional transformation could be ascribed to two factors: (1) thermodynamically, there was a huge activation energy involved in the transformation process from the $MAPbI_3$ 3D perovskite to $ODAPbI_4$ 2D perovskite, although the anti-*gauche* isomerization of ODA may increase the Gibbs free energy of the $ODAPbI_4$ 2D perovskite (still lower than that of $MAPbI_3$); (2) kinetically, the transition from 3D to 2D perovskite occurred too slowly to be observed within a 10-second post-treatment time. This study emphasized the importance of reasonable molecular design for the surface modification and bulk passivation of perovskites (Fig. 11k).

3.3.3. Alicyclic spacers. In contrast to aromatic compounds, which also have a ring structure, alicyclic spacers, such as cyclohexylammonium, exhibit stronger N–H bonding due to the localized electron density in the cycle structure. The stronger bonding is more favorable for defect passivation compared to aromatic spacers such as phenylammonium.[116,117] As a result, in addition to long-chain aliphatic compounds, alicyclic spacer cations have been found to be suitable for producing 2D/3D heterojunctions.[118,119] For example, in 2022, Wu's group applied an alicyclic organic salt called (*R*)-(−)-1-cyclohexylethylammonium iodide (*R*-CEAI) to fabricate multiple 2D/3D perovskite homojunctions using the DGPF method.[120] Grazing incidence X-ray diffraction (GIXRD) characterization revealed residual stress in the *R*-CEAI-based perovskite films. The alleviated lattice distortion resulting from this stress was beneficial for carrier dynamics and device performance. Consequently, an *R*-CEAI-based PSC showed an improved PCE of 22.52% in comparison with the pristine PSC with a lower PCE of 19.43%.

In particular, the formation of coexisting 2D/3D heterojunctions opens up the possibility of combining different types of organic spacers. For instance, in 2022, Mai *et al.* selected oleylammonium (OAm) and PEA as perovskite bulk and surface passivation agents, respectively. These agents not only promoted the crystal growth in the out-of-plane orientation but also passivated defects at grain boundaries and the perovskite surface, leading to a reduction in trap density and nonradiative recombination.[121] Consequently, the modified 2D/3D hybrid device with the architecture of FTO/NiO_x/PTAA/Al_2O_3/perovskite/PCBM/BCP/Ag achieved a PCE of 20.52% without any hysteresis. More reported organic spacer cations applied in bulk incorporation and surface treatment coexisting type PSCs can be found in Table 3.

3.4. Other models

In addition to the three mainstream 2D/3D heterojunction structures mentioned above, 2D perovskites can also be constructed at the bottom of 3D perovskites through self-assembly and/or *in situ* formation to passivate the defects of the buried interface in 3D PSCs.[128] Yu *et al.* achieved this by fabricating 2D perovskite *in situ* at the buried interface through the interaction between the PEA spacers and 3D perovskite. They first deposited PEABr on an ITO substrate and then spin-coated the perovskite precursor. Moreover, Chen *et al.* demonstrated that the introduction of chiral cations, namely α-methylbenzylamine (S-/R-/rac-MBA), can induce the formation of 2D perovskites at the interface between PEDOT:PSS and $FASnI_3$, resulting in better matched energy levels and improved interface contacts and leading to improved hole extraction from $FASnI_3$ by

Table 3 An exhaustive list of recently reported organic spacer cations applied in bulk incorporation and surface treatment coexisting type PSCs

Spcers	Device architecture	V_{OC} (V)	FF (%)	J_{SC} (mA cm^{-2})	PCE (%)	Ref.
FPEA	ITO/PEDOT:PSS/$FASnI_3$/ICBA/BCP/Al	0.840	70.76	24.91	14.81	115
2-PyEA	ITO/SnO_2/$FA_{0.92}MA_{0.08}PbI_3$/spiro-OMeTAD/Au	1.140	82.10	24.80	23.20	111
DMA	FTO/TiO_2/$Cs_{0.05}FA_{0.85}MA_{0.10}Pb(I_{0.97}Br_{0.03})_3$/spiro-OMeTAD/$MoO_3$/Ag	1.140	78.00	25.43	22.61	122
ThFA	ITO/SnO_2/$FA_{0.84}MA_{0.16}PbI_3$/spiro-OMeTAD/MoO_3/Ag	1.210	81.62	25.07	24.69	112
BA	ITO/SnO_2/$Cs_{0.03}(FA_{0.97}MA_{0.03})_{0.97}Pb(I_{0.97}Br_{0.03})_3$/spiro-OMeTAD/Au	1.210	80.00	24.57	23.78	113
OA	FTO/c-TiO_2/PMMA:PCBM/$Cs_{0.07}Rb_{0.03}FA_{0.765}MA_{0.135}PbI_{2.55}Br_{0.45}$/spiro-OMeTAD/Au	1.240	78.46	24.24	23.62	123
TBA	FTO/PEDOT:PSS/$FAPbI_3$/spiro-OMeTAD/Au	0.990	71.20	24.23	17.02	124
CME	FTO/c-TiO_2/m-TiO_2/$Cs_{0.05}FA_{0.80}MA_{0.15}Pb(I_{0.85}Br_{0.15})_3$/spiro-OMeTAD/Au	1.110	77.00	23.45	20.33	125
Gu	ITO/SnO_2/$(FA_{0.93}MA_{0.07}Pb(I_{0.93}Br_{0.07})_3$/spiro-OMeTAD/Au	1.120	81.15	24.79	22.53	126
TBH	$(FAPbI_3)_{0.84}(CsPbI_3)_{0.06}(MAPbBr_3)_{0.10}$	1.186	84.10	22.60	22.54	127
R-CEA	FTO/TiO_2/$(FAPbI_3)_{0.84}(CsPbI_3)_{0.05}(MAPbBr_3)_{0.11}$/spiro-OMeTAD/Au	1.195	80.50	23.42	22.52	120
BDA	ITO/Cu:NiO_X/$MAPbI_3$/PCBM/C_{60}/Ag	1.110	76.00	14.48	11.97	114
EDBE	ITO/Cu:NiO_X/$MAPbI_3$/PCBM/C_{60}/Ag	1.160	71.00	4.33	3.44	114

PEDOT:PSS.[129] To achieve this, MBA was added in advance to prepare a quasi-2D perovskite precursor with n = 5. The precursor primarily formed a 3D structure from the upper surface rather than quasi-2D perovskite when the anti-solvent was dropped, due to the lower formation energy of 3D perovskite. Subsequently, the MBA molecules acted as templates to guide the downward growth of 3D perovskite. Finally, at the end of solvent evaporation, the excess MBA spacers interacted with $[PbI_6]^{4-}$ octahedron layers at the bottom of the 3D perovskite, thus forming a 2D perovskite at the buried bottom interface. Additionally, considering the significance of buried interface passivation, White *et al.* proposed a design of 2D/3D/2D structure for double-side surface modification using the BA spacer, achieving in a remarkable PCE of 22.77%.[130] These studies have some implications for constructing 2D perovskites at the buried interface to reduce buried interface defects and enhance charge extraction.

4. Summary and outlook

In the past several years, significant advancements have been made in constructing 2D/3D heterojunctions by incorporating bulky and hydrophobic organic spacers into or onto 3D perovskite films. These advancements aim to enhance the photovoltaic performance and long-term stability of PSCs. However, due to the lack of a deep understanding in this field, we have presented the structural characteristics of both 3D and 2D perovskite materials, discussed the transformation process from 3D to 2D perovskite, summarized the key organic spacers used in fabricating 2D/3D PSCs, highlighted their roles in the formation mechanisms of different types of 2D/3D heterojunctions, and drawn the following conclusions:

2D/3D heterojunctions can be fabricated through bulk incorporation and surface treatment methods. In the bulk incorporation process, the formed 2D/3D heterojunctions play several roles: (1) passivating defects in bulk of 3D perovskite; (2) forming a distinctive structure, such as a porous structure for the PbI_2 film; (3) providing seeds and serving as a template to assist 3D perovskite growth; and (4) regulating the crystallization rate and controlling the crystal orientation; and (5) forming type I heterojunctions and reducing carrier recombination at grain boundaries. On the other hand, in the surface treatment process, 2D components containing different organic spacers are deposited on top of 3D perovskite through post-treatment. The resulting 2D/3D heterojunctions formed by this method exhibit the following effects: (1) passivating defects on the perovskite film surface; (2) forming a hydrophobic capping layer to improve humidity stability; (3) inhibiting ion migration; and (4) generating type II heterojunctions to promote carrier transport. Furthermore, some researchers have combined these two methods to prepare coexisting 2D/3D heterojunctions, which offer advantages of both types of 2D/3D heterojunctions.

Looking ahead, the construction of 2D/3D heterostructures remains a crucial method to improve the comprehensive performance of PSCs, including high efficiency and long-term stability. While the stability of 2D/3D hybrid PSCs is higher than that of 3D PSCs, the maximum PCE of 2D/3D hybrid PSCs (PCE = 24.9%)[30] is still behind that of the 3D PSCs (PCE = 26.1%).[2] To bridge this efficiency gap, researchers need to dedicate more attention and efforts. Based on the contents of this review, we propose several possible strategies for enhancing 2D/3D hybrid PSCs. (1) Prioritizing aromatic spacers over aliphatic spacers: aromatic spacers possess π-conjugated structures with a higher dielectric constant, which benefits charge transfer. (2) Focusing on modifying 2D seed crystals rather than simple salt treatments: recent studies have shown that 2D seed crystals provide more advantages compared to salt treatments alone. (3) Developing a coexisting 2D/3D heterojunction model instead of a single 2D/3D heterojunction model: as described in this review, the coexisting 2D/3D heterojunction model can take advantages of the two other single models. (4) Constructing 2D/3D heterojunctions in perovskite solar modules or tandem solar cells: in order to realize commercialization, the preparation of the perovskite solar modules and tandem solar cells is an inevitable trend for the future. Therefore, further studies are necessary to develop preparation technologies for constructing 2D/3D heterojunctions in perovskite solar modules and tandem solar cells.

In conclusion, we believe that with the joint efforts of researchers, significant progress can be made in improving the efficiency and stability of 2D/3D PSCs, ultimately leading to their commercialization.

Conflicts of interest

There are no conflicts to declare.

Acknowledgements

This work was financially supported by the National Natural Science Foundation of China (Grant No. 52273182) and Natural Science Foundation of Hebei Province of China (Grant No. B2022408005).

References

1 A. Kojima, K. Teshima, Y. Shirai and T. Miyasaka, Organometal Halide Perovskites as Visible-Light Sensitizers for Photovoltaic Cells, *J. Am. Chem. Soc.*, 2009, **131**, 6050–6051.
2 NREL, Best Research-Cell Efficiencies, **https://www.nrel.gov/pv/cell-efficiency.html**, access on 30 August 2023.
3 C. Wehrenfennig, G. E. Eperon, M. B. Johnston, H. J. Snaith and L. M. Herz, High Charge Carrier Mobilities and Lifetimes in Organolead Trihalide Perovskites, *Adv. Mater.*, 2014, **26**, 1584–1589.
4 L. N. Li, X. Y. Shang, S. S. Wang, N. N. Dong, C. M. Ji, X. Y. Chen, S. E. Zhao, J. Wang, Z. H. Sun, M. C. Hong and J. H. Luo, Bilayered Hybrid Perovskite Ferroelectric with

Giant Two-Photon Absorption, *J. Am. Chem. Soc.*, 2018, **140**, 6806–6809.

5 D. Stranks Samuel, E. Eperon Giles, G. Grancini, C. Menelaou, J. P. Alcocer Marcelo, T. Leijtens, M. Herz Laura, A. Petrozza and J. Snaith Henry, Electron-Hole Diffusion Lengths Exceeding 1 Micrometer in an Organometal Trihalide Perovskite Absorber, *Science*, 2013, **342**, 341–344.

6 G. Xing, N. Mathews, S. Sun, S. S. Lim, Y. M. Lam, M. Grätzel, S. Mhaisalkar and T. C. Sum, Long-Range Balanced Electron- and Hole-Transport Lengths in Organic-Inorganic $CH_3NH_3PbI_3$, *Science*, 2013, **342**, 344–347.

7 M. Baranowski and P. Plochocka, Excitons in Metal-Halide Perovskites, *Adv. Energy Mater.*, 2020, **10**, 1903659.

8 R. Chen, Y. Hui, B. Wu, Y. Wang, X. Huang, Z. Xu, P. Ruan, W. Zhang, F. Cheng, W. Zhang, J. Yin, J. Li and N. Zheng, Moisture-tolerant and high-quality α-$CsPbI_3$ films for efficient and stable perovskite solar modules, *J. Mater. Chem. A*, 2020, **8**, 9597–9606.

9 Q. Sun, P. Fassl, D. Becker-Koch, A. Bausch, B. Rivkin, S. Bai, P. E. Hopkinson, H. J. Snaith and Y. Vaynzof, Role of Microstructure in Oxygen Induced Photodegradation of Methylammonium Lead Triiodide Perovskite Films, *Adv. Energy Mater.*, 2017, **7**, 1700977.

10 D. B. Khadka, Y. Shirai, M. Yanagida, K. Uto and K. Miyano, Analysis of degradation kinetics of halide perovskite solar cells induced by light and heat stress, *Sol. Energy Mater. Sol. Cells*, 2022, **246**, 111899.

11 G. Abdelmageed, L. Jewell, K. Hellier, L. Seymour, B. Luo, F. Bridges, J. Z. Zhang and S. Carter, Mechanisms for light induced degradation in $MAPbI_3$ perovskite thin films and solar cells, *Appl. Phys. Lett.*, 2016, **109**, 233905.

12 B. Rivkin, P. Fassl, Q. Sun, A. D. Taylor, Z. Chen and Y. Vaynzof, Effect of Ion Migration-Induced Electrode Degradation on the Operational Stability of Perovskite Solar Cells, *ACS Omega*, 2018, **3**, 10042–10047.

13 Y. Gao, R. Wang and Y. Liu, Progress of Two-dimensional Perovskite Solar Cells Based on Aromatic Organic Spacers, *Chin. J. Lumin.*, 2023, **44**, 449–465.

14 I. C. Smith, E. T. Hoke, D. Solis-Ibarra, M. D. McGehee and H. I. Karunadasa, A layered hybrid perovskite solar-cell absorber with enhanced moisture stability, *Angew. Chem., Int. Ed.*, 2014, **53**, 11232–11235.

15 H. Lai, B. Kan, T. Liu, N. Zheng, Z. Xie, T. Zhou, X. Wan, X. Zhang, Y. Liu and Y. Chen, Two-Dimensional Ruddlesden-Popper Perovskite with Nanorod-like Morphology for Solar Cells with Efficiency Exceeding 15, *J. Am. Chem. Soc.*, 2018, **140**, 11639–11646.

16 D. Lu, G. Lv, Z. Xu, Y. Dong, X. Ji and Y. Liu, Thiophene-Based Two-Dimensional Dion-Jacobson Perovskite Solar Cells with over 15% Efficiency, *J. Am. Chem. Soc.*, 2020, **142**, 11114–11122.

17 Q. Li, Y. Dong, G. Lv, T. Liu, D. Lu, N. Zheng, X. Dong, Z. Xu, Z. Xie and Y. Liu, Fluorinated Aromatic Formamidinium Spacers Boost Efficiency of Layered Ruddlesden–Popper Perovskite Solar Cells, *ACS Energy Lett.*, 2021, **6**, 2072–2080.

18 R. Wang, X. Dong, Q. Ling, Q. Fu, Z. Hu, Z. Xu, H. Zhang, Q. Li and Y. Liu, Spacer Engineering for 2D Ruddlesden–Popper Perovskites with an Ultralong Carrier Lifetime of Over 18 μs Enable Efficient Solar Cells, *ACS Energy Lett.*, 2022, **7**, 3656–3665.

19 Y. Zhang and N.-G. Park, Quasi-Two-Dimensional Perovskite Solar Cells with Efficiency Exceeding 22%, *ACS Energy Lett.*, 2022, **7**, 757–765.

20 D. Li, Z. Xing, X. Meng, X. Hu, T. Hu and Y. Chen, Selection of Functional Spacer Cations for Efficient 2D/3D Perovskite Solar Cells, *CCS Chem.*, 2023, **5**, 781–801.

21 G. Grancini and M. K. Nazeeruddin, Dimensional tailoring of hybrid perovskites for photovoltaics, *Nat. Rev. Mater.*, 2018, **4**, 4–22.

22 W. Travis, E. N. K. Glover, H. Bronstein, D. O. Scanlon and R. G. Palgrave, On the application of the tolerance factor to inorganic and hybrid halide perovskites: a revised system, *Chem. Sci.*, 2016, **7**, 4548–4556.

23 A. Krishna, S. Gottis, M. K. Nazeeruddin and F. Sauvage, Mixed Dimensional 2D/3D Hybrid Perovskite Absorbers: The Future of Perovskite Solar Cells?, *Adv. Funct. Mater.*, 2019, **29**, 1806482.

24 Y.-T. Li, L. Han, H. Liu, K. Sun, D. Luo, X.-L. Guo, D.-L. Yu and T.-L. Ren, Review on Organic–Inorganic Two-Dimensional Perovskite-Based Optoelectronic Devices, *ACS Appl. Electron. Mater.*, 2022, **4**, 547–567.

25 Y. Xu, M. Wang, Y. Lei, Z. Ci and Z. Jin, Crystallization Kinetics in 2D Perovskite Solar Cells, *Adv. Energy Mater.*, 2020, **10**, 2002558.

26 L. Yan, J. Ma, P. Li, S. Zang, L. Han, Y. Zhang and Y. Song, Charge-Carrier Transport in Quasi-2D Ruddlesden–Popper Perovskite Solar Cells, *Adv. Mater.*, 2022, **34**, 2106822.

27 Z. Wang, Q. Lin, F. P. Chmiel, N. Sakai, L. M. Herz and H. J. Snaith, Efficient ambient-air-stable solar cells with 2D–3D heterostructured butylammonium-caesium-formamidinium lead halide perovskites, *Nat. Energy*, 2017, **2**, 17135.

28 J. W. Lee, Z. Dai, T. H. Han, C. Choi, S. Y. Chang, S. J. Lee, N. De Marco, H. Zhao, P. Sun, Y. Huang and Y. Yang, 2D perovskite stabilized phase-pure formamidinium perovskite solar cells, *Nat. Commun.*, 2018, **9**, 3021.

29 C. Luo, G. Zheng, F. Gao, X. Wang, Y. Zhao, X. Gao and Q. Zhao, Facet orientation tailoring via 2D-seed- induced growth enables highly efficient and stable perovskite solar cells, *Joule*, 2022, **6**, 240–257.

30 T. Yang, C. Ma, W. Cai, S. Wang, Y. Wu, J. Feng, N. Wu, H. Li, W. Huang, Z. Ding, L. Gao, S. Liu and K. Zhao, Amidino-based Dion-Jacobson 2D perovskite for efficient and stable 2D/3D heterostructure perovskite solar cells, *Joule*, 2023, **7**, 574–586.

31 X. Zheng, Y. Hou, C. Bao, J. Yin, F. Yuan, Z. Huang, K. Song, J. Liu, J. Troughton, N. Gasparini, C. Zhou, Y. Lin, D.-J. Xue, B. Chen, A. K. Johnston, N. Wei, M. N. Hedhili, M. Wei, A. Y. Alsalloum, P. Maity, B. Turedi, C. Yang, D. Baran, T. D. Anthopoulos, Y. Han, Z.-H. Lu, O. F. Mohammed, F. Gao, E. H. Sargent and O. M. Bakr, Managing grains and interfaces via ligand anchoring enables 22.3%-efficiency

inverted perovskite solar cells, *Nat. Energy*, 2020, **5**, 131–140.

32 Y. Liu, S. Akin, L. Pan, R. Uchida, N. Arora, J. V. Milić, A. Hinderhofer, F. Schreiber, A. R. Uhl, S. M. Zakeeruddin, A. Hagfeldt, M. I. Dar and M. Grätzel, Ultrahydrophobic 3D/2D fluoroarene bilayer-based water-resistant perovskite solar cells with efficiencies exceeding 22%, *Sci. Adv.*, 2019, **5**, eaaw2543.

33 A. H. Proppe, M. Wei, B. Chen, R. Quintero-Bermudez, S. O. Kelley and E. H. Sargent, Photochemically Cross-Linked Quantum Well Ligands for 2D/3D Perovskite Photovoltaics with Improved Photovoltage and Stability, *J. Am. Chem. Soc.*, 2019, **141**, 14180–14189.

34 Y.-W. Jang, S. Lee, K. M. Yeom, K. Jeong, K. Choi, M. Choi and J. H. Noh, Intact 2D/3D halide junction perovskite solar cells via solid-phase in-plane growth, *Nat. Energy*, 2021, **6**, 63–71.

35 A. H. Proppe, A. Johnston, S. Teale, A. Mahata, R. Quintero-Bermudez, E. H. Jung, L. Grater, T. Cui, T. Filleter, C. Y. Kim, S. O. Kelley, F. De Angelis and E. H. Sargent, Multication perovskite 2D/3D interfaces form via progressive dimensional reduction, *Nat. Commun.*, 2021, **12**, 3472.

36 Y. Du, D. Zhu, Q. Cai, S. Yuan, G. Shen, P. Dong, C. Mu, Y. Wang and X.-C. Ai, Spacer Engineering of Thiophene-Based Two-Dimensional/Three-Dimensional Hybrid Perovskites for Stable and Efficient Solar Cells, *J. Phys. Chem. C*, 2022, **126**, 3351–3358.

37 M.-H. Li, H.-H. Yeh, Y.-H. Chiang, U. S. Jeng, C.-J. Su, H.-W. Shiu, Y.-J. Hsu, N. Kosugi, T. Ohigashi, Y.-A. Chen, P.-S. Shen, P. Chen and T.-F. Guo, Highly Efficient 2D/3D Hybrid Perovskite Solar Cells via Low-Pressure Vapor-Assisted Solution Process, *Adv. Mater.*, 2018, **30**, 1801401.

38 M.-G. La-Placa, L. Gil-Escrig, D. Guo, F. Palazon, T. J. Savenije, M. Sessolo and H. J. Bolink, Vacuum-Deposited 2D/3D Perovskite Heterojunctions, *ACS Energy Lett.*, 2019, **4**, 2893–2901.

39 D. S. Lee, J. S. Yun, J. Kim, A. M. Soufiani, S. Chen, Y. Cho, X. Deng, J. Seidel, S. Lim, S. Huang and A. W. Y. Ho-Baillie, Passivation of Grain Boundaries by Phenethylammonium in Formamidinium-Methylammonium Lead Halide Perovskite Solar Cells, *ACS Energy Lett.*, 2018, **3**, 647–654.

40 T. Liu, J. Guo, D. Lu, Z. Xu, Q. Fu, N. Zheng, Z. Xie, X. Wan, X. Zhang, Y. Liu and Y. Chen, Spacer Engineering Using Aromatic Formamidinium in 2D/3D Hybrid Perovskites for Highly Efficient Solar Cells, *ACS Nano*, 2021, **15**, 7811–7820.

41 T. Zhou, Z. Xu, R. Wang, X. Dong, Q. Fu and Y. Liu, Crystal Growth Regulation of 2D/3D Perovskite Films for Solar Cells with Both High Efficiency and Stability, *Adv. Mater.*, 2022, **34**, e2200705.

42 F. Yang, P. Zhang, M. A. Kamarudin, G. Kapil, T. Ma and S. Hayase, Addition Effect of Pyreneammonium Iodide to Methylammonium Lead Halide Perovskite-2D/3D Heterostructured Perovskite with Enhanced Stability, *Adv. Funct. Mater.*, 2018, **28**, 1804856.

43 T. Zhou, H. Lai, T. Liu, D. Lu, X. Wan, X. Zhang, Y. Liu and Y. Chen, Highly Efficient and Stable Solar Cells Based on Crystalline Oriented 2D/3D Hybrid Perovskite, *Adv. Mater.*, 2019, **31**, e1901242.

44 Y. Li, J. Wu, Y. Zhang, L. Zhang, X. Zhou, B. Hu, Z. Jiang, J. Zeng, D. Wang, Y. Liu, S. Chen, Z. Liu, C. Liu, X. Wang and B. Xu, Whether organic spacer cations induced 2D/3D or quasi-2D/3D mixed dimensional perovskites?, *Chem. Eng. J.*, 2022, **450**, 137887.

45 Y. Chen, Y. Sun, J. Peng, W. Zhang, X. Su, K. Zheng, T. Pullerits and Z. Liang, Tailoring Organic Cation of 2D Air-Stable Organometal Halide Perovskites for Highly Efficient Planar Solar Cells, *Adv. Energy Mater.*, 2017, **7**, 1700162.

46 X. Zhang, X. Ren, B. Liu, R. Munir, X. Zhu, D. Yang, J. Li, Y. Liu, D.-M. Smilgies, R. Li, Z. Yang, T. Niu, X. Wang, A. Amassian, K. Zhao and S. Liu, Stable high efficiency two-dimensional perovskite solar cells via cesium doping, *Energy Environ. Sci.*, 2017, **10**, 2095–2102.

47 N. Zhou, Y. Shen, L. Li, S. Tan, N. Liu, G. Zheng, Q. Chen and H. Zhou, Exploration of Crystallization Kinetics in Quasi Two-Dimensional Perovskite and High Performance Solar Cells, *J. Am. Chem. Soc.*, 2018, **140**, 459–465.

48 B.-w Park, H. W. Kwon, Y. Lee, D. Y. Lee, M. G. Kim, G. Kim, K.-j Kim, Y. K. Kim, J. Im, T. J. Shin and S. I. Seok, Stabilization of formamidinium lead triiodide α-phase with isopropylammonium chloride for perovskite solar cells, *Nat. Energy*, 2021, **6**, 419–428.

49 S. Sandhu, R. Singh, K. Yoo, M. Kumar and J.-J. Lee, Effect of binary additives in mixed 2D/3D Sn-based perovskite solar cells, *J. Power Sources*, 2021, **491**, 229574.

50 Y. Zhong, G. Liu, Y. Su, W. Sheng, L. Gong, J. Zhang, L. Tan and Y. Chen, Diammonium Molecular Configuration-Induced Regulation of Crystal Orientation and Carrier Dynamics for Highly Efficient and Stable 2D/3D Perovskite Solar Cells, *Angew. Chem., Int. Ed.*, 2022, **61**, e202114588.

51 S.-C. Yun, S. Ma, H.-C. Kwon, K. Kim, G. Jang, H. Yang and J. Moon, Amino acid salt-driven planar hybrid perovskite solar cells with enhanced humidity stability, *Nano Energy*, 2019, **59**, 481–491.

52 H. Zheng, X. Dong, W. Wu, G. Liu and X. Pan, Multifunctional Heterocyclic-Based Spacer Cation for Efficient and Stable 2D/3D Perovskite Solar Cells, *ACS Appl. Mater. Interfaces*, 2022, **14**, 9183–9191.

53 N. Zhou, Y. Zhang, Z. Huang, Z. Guo, C. Zhu, J. He, Q. Chen, W. Sun and H. Zhou, Mobile Media Promotes Orientation of 2D/3D Hybrid Lead Halide Perovskite for Efficient Solar Cells, *ACS Nano*, 2021, **15**, 8350–8362.

54 G. Liu, H. Zheng, X. Xu, L.-Z. Zhu, X. Zhang and X. Pan, Design of High-Efficiency and Environmentally Stable Mixed-Dimensional Perovskite Solar Cells Based on Cesium-Formamidinium Lead Halide Component, *Chem. Mater.*, 2018, **30**, 7691–7698.

55 J. Xu, J. Cui, S. Yang, Z. Liu, X. Guo, Y. Che, D. Xu, W. Zhao, N. Yuan, J. Ding and S. Liu, Stable High-Efficiency $CsPbI_2Br$ Solar Cells by Designed Passivation Using Multifunctional 2D Perovskite, *Adv. Funct. Mater.*, 2022, **32**, 2202829.

56 Z. Wang, Y. Lu, Z. Xu, J. Hu, Y. Chen, C. Zhang, Y. Wang, F. Guo and Y. Mai, An Embedding 2D/3D Heterostructure Enables High-Performance FA-Alloyed Flexible Perovskite Solar Cells with Efficiency over 20, *Adv. Sci.*, 2021, **8**, e2101856.

57 Y. Li, J. Zhang, J. Xiang, H. Hu, H. Zhong and Y. Shi, A Novel 4,4'-Bipiperidine-Based Organic Salt for Efficient and Stable 2D-3D Perovskite Solar Cells, *ACS Appl. Mater. Interfaces*, 2022, **14**, 22324–22331.

58 G. Wu, R. Liang, M. Ge, G. Sun, Y. Zhang and G. Xing, Surface Passivation Using 2D Perovskites toward Efficient and Stable Perovskite Solar Cells, *Adv. Mater.*, 2022, **34**, e2105635.

59 Y. Hu, J. Schlipf, M. Wussler, M. L. Petrus, W. Jaegermann, T. Bein, P. Muller-Buschbaum and P. Docampo, Hybrid Perovskite/Perovskite Heterojunction Solar Cells, *ACS Nano*, 2016, **10**, 5999–6007.

60 C. Ma, C. Leng, Y. Ji, X. Wei, K. Sun, L. Tang, J. Yang, W. Luo, C. Li, Y. Deng, S. Feng, J. Shen, S. Lu, C. Du and H. Shi, 2D/3D perovskite hybrids as moisture-tolerant and efficient light absorbers for solar cells, *Nanoscale*, 2016, **8**, 18309–18314.

61 G. Grancini, C. Roldan-Carmona, I. Zimmermann, E. Mosconi, X. Lee, D. Martineau, S. Narbey, F. Oswald, F. De Angelis, M. Graetzel and M. K. Nazeeruddin, One-Year stable perovskite solar cells by 2D/3D interface engineering, *Nat. Commun.*, 2017, **8**, 15684.

62 P. Chen, Y. Bai, S. Wang, M. Lyu, J. H. Yun and L. Wang, In Situ Growth of 2D Perovskite Capping Layer for Stable and Efficient Perovskite Solar Cells, *Adv. Funct. Mater.*, 2018, **28**, 1706923.

63 F. Cao, H. Chen, S. Wang, P. Chen, C. Zhu, Z. Lan, W. Sun, Y. Li and J. Wu, One-step constructed dual interfacial layers for stable perovskite solar cells, *Mater. Today Phys.*, 2022, **27**, 100796.

64 Y. Liu, B. J. Kim, H. Wu, G. Boschloo and E. M. J. Johansson, Efficient and Stable $FAPbBr_3$ Perovskite Solar Cells via Interface Modification by a Low-Dimensional Perovskite Layer, *ACS Appl. Energy Mater.*, 2021, **4**, 9276–9282.

65 Y. Lv, Y. Shi, X. Song, J. Liu, M. Wang, S. Wang, Y. Feng, S. Jin and C. Hao, Bromine Doping as an Efficient Strategy to Reduce the Interfacial Defects in Hybrid Two-Dimensional/Three-Dimensional Stacking Perovskite Solar Cells, *ACS Appl. Mater. Interfaces*, 2018, **10**, 31755–31764.

66 H. Kim, M. Pei, Y. Lee, A. A. Sutanto, S. Paek, V. I. E. Queloz, A. J. Huckaba, K. T. Cho, H. J. Yun, H. Yang and M. K. Nazeeruddin, Self-Crystallized Multifunctional 2D Perovskite for Efficient and Stable Perovskite Solar Cells, *Adv. Funct. Mater.*, 2020, **30**, 1910620.

67 C. Ji, C. Liang, Q. Song, H. Gong, N. Liu, F. You, D. Li and Z. He, Interface Engineering of 2D/3D Perovskite Heterojunction Improves Photovoltaic Efficiency and Stability, *Solar RRL*, 2021, **5**, 2100072.

68 Y. Yu, R. Liu, C. Liu, T. Hou, Q. Wu, M. Zhang and H. Yu, Dimensional Engineering Enables 1.31 V Open-Circuit Voltage for Efficient and Stable Wide-Bandgap Halide Perovskite Solar Cells, *Solar RRL*, 2022, **6**, 2200021.

69 Q. Zhou, L. Liang, J. Hu, B. Cao, L. Yang, T. Wu, X. Li, B. Zhang and P. Gao, High-Performance Perovskite Solar Cells with Enhanced Environmental Stability Based on a $(p\text{-}FC_6H_4C_2H_4NH_3)_2[PbI_4]$ Capping Layer, *Adv. Energy Mater.*, 2019, **9**, 1802595.

70 R. Garai, R. K. Gupta, M. Hossain and P. K. Iyer, Surface recrystallized stable 2D–3D graded perovskite solar cells for efficiency beyond 21%, *J. Mater. Chem. A*, 2021, **9**, 26069–26076.

71 H. Yu, F. Xu, C. Li, B. Yuan, T. Liu, Z. Pan, Y. Zhou and B. Cao, In-situ fluorinated 2D/3D invert perovskite film solar cell with enhanced ambient stability, *Sol. Energy*, 2021, **221**, 583–590.

72 Y. Cai, J. Wen, Z. Liu, F. Qian, C. Duan, K. He, W. Zhao, S. Zhan, S. Yang, J. Cui and S. Liu, Graded 2D/3D $(CF_3\text{-}PEA)_2FA_{0.85}MA_{0.15}Pb_2I_7/FA_{0.85}MA_{0.15}PbI_3$ heterojunction for stable perovskite solar cell with an efficiency over 23.0%, *J. Energy Chem.*, 2022, **65**, 480–489.

73 H. Ran, L. Cao, Y. Zhao, M. Chen, P. Qi, H. Wu, Y. Lu, Y. Zhang, S. Wang and Y. Tang, Constructing 2D passivation layer on perovskites based on 3-chlorobenzylamine enables efficient and stable perovskite solar cells, *J. Alloys Compd.*, 2022, **926**, 166891.

74 M. D. Malouangou, Y. Zhang, Y. Yang, M. T. Mbumba, M. W. Akram, E. Rop, J. Tsiba Matondo and M. Guli, Enhancing the efficiency and stability of 2D-3D perovskite solar cells with embedded interface passivation with diammonium cation spacer, *Sol. Energy Mater. Sol. Cells*, 2023, **251**, 112135.

75 W. H. Rodebush and I. Feldman, Ultraviolet Absorption Spectra of Organic Molecules. III. Mechanical Interference of Substituent Groups with Resonance Configurations, *J. Am. Chem. Soc.*, 1946, **68**, 896–899.

76 J.-P. Deng, W.-T. Yang and B. Rånby, Auto-Initiating Performance of Styrene on Surface Photografting Polymerization, *Macromol. Rapid Commun.*, 2001, **22**, 535–538.

77 C. Chen, J. Liang, J. Zhang, X. Liu, X. Yin, H. Cui, H. Wang, C. Wang, Z. Li, J. Gong, Q. Lin, W. Ke, C. Tao, B. Da, Z. Ding, X. Xiao and G. Fang, Interfacial engineering of a thiophene-based 2D/3D perovskite heterojunction for efficient and stable inverted wide-bandgap perovskite solar cells, *Nano Energy*, 2021, **90**, 106608.

78 A. A. Sutanto, P. Caprioglio, N. Drigo, Y. J. Hofstetter, I. Garcia-Benito, V. I. E. Queloz, D. Neher, M. K. Nazeeruddin, M. Stolterfoht, Y. Vaynzof and G. Grancini, 2D/3D perovskite engineering eliminates interfacial recombination losses in hybrid perovskite solar cells, *Chem*, 2021, **7**, 1903–1916.

79 A. A. Sutanto, N. Drigo, V. I. E. Queloz, I. Garcia-Benito, A. R. Kirmani, L. J. Richter, P. A. Schouwink, K. T. Cho, S. Paek, M. K. Nazeeruddin and G. Grancini, Dynamical evolution of the 2D/3D interface: a hidden driver behind perovskite solar cell instability, *J. Mater. Chem. A*, 2020, **8**, 2343–2348.

80 Y. Huang, Z. Yuan, J. Yang, S. Yin, A. Liang, G. Xie, C. Feng, Z. Zhou, Q. Xue, Y. Pan, F. Huang and Y. Chen, Highly efficient perovskite solar cells by building 2D/3D perovskite heterojuction in situ for interfacial passivation and energy level adjustment, *Sci. China: Chem.*, 2023, **66**, 449–458.

81 W. Zhou, L. Jia, M. Chen, X. Li, Z. Su, Y. Shang, X. Jiang, X. Gao, T. Chen, M. Wang, Z. Zhu, Y. Lu and S. Yang, An Improbable Amino-Functionalized Fullerene Spacer Enables 2D/3D Hybrid Perovskite with Enhanced Electron Transport in Solar Cells, *Adv. Funct. Mater.*, 2022, **32**, 2201374.

82 Q. Wang, F. Lin, C.-C. Chueh, T. Zhao, M. Eslamian and A. K. Y. Jen, Enhancing efficiency of perovskite solar cells by reducing defects through imidazolium cation incorporation, *Mater. Today Energy*, 2018, **7**, 161–168.

83 J. Kim, T. Hwang, B. Lee, S. Lee, K. Park, H. H. Park and B. Park, An Aromatic Diamine Molecule as the A-Site Solute for Highly Durable and Efficient Perovskite Solar Cells, *Small Methods*, 2019, **3**, 1800361.

84 C. Wang, X. Wang, Z. He, B. Zhou, D. Qu, Y. Wang, H. Hu, Q. Hu and Y. Tu, Minimizing voltage deficit in Methylammonium-Free perovskite solar cells via surface reconstruction, *Chem. Eng. J.*, 2022, **444**, 136622.

85 I. Zimmermann, S. Aghazada and M. K. Nazeeruddin, Lead and HTM Free Stable Two-Dimensional Tin Perovskites with Suitable Band Gap for Solar Cell Applications, *Angew. Chem., Int. Ed.*, 2019, **58**, 1072–1076.

86 Q. Li, Q. Shu, Y. Wang, D.-Y. Zhou, F. Wang, Q. Yuan, S. Yi, H. Wang and L. Feng, Interfacial Engineering by In Situ Building of a 3D/2D Heterojunction for Inverted $CsPbI_2Br$ Solar Cells: Beyond Moisture Proof, *ACS Appl. Energy Mater.*, 2021, **4**, 10081–10090.

87 K. Wojciechowski, T. Leijtens, S. Siprova, C. Schlueter, M. T. Horantner, J. T. Wang, C. Z. Li, A. K. Jen, T. L. Lee and H. J. Snaith, C60 as an Efficient n-Type Compact Layer in Perovskite Solar Cells, *J. Phys. Chem. Lett.*, 2015, **6**, 2399–2405.

88 Y. Shao, Z. Xiao, C. Bi, Y. Yuan and J. Huang, Origin and elimination of photocurrent hysteresis by fullerene passivation in $CH_3NH_3PbI_3$ planar heterojunction solar cells, *Nat. Commun.*, 2014, **5**, 5784.

89 Y. Bai, Q. Dong, Y. Shao, Y. Deng, Q. Wang, L. Shen, D. Wang, W. Wei and J. Huang, Enhancing stability and efficiency of perovskite solar cells with crosslinkable silane-functionalized and doped fullerene, *Nat. Commun.*, 2016, **7**, 12806.

90 Y. Li, Y. Zhao, Q. Chen, Y. M. Yang, Y. Liu, Z. Hong, Z. Liu, Y. T. Hsieh, L. Meng, Y. Li and Y. Yang, Multifunctional Fullerene Derivative for Interface Engineering in Perovskite Solar Cells, *J. Am. Chem. Soc.*, 2015, **137**, 15540.

91 W. Chi and S. K. Banerjee, Engineering strategies for two-dimensional perovskite solar cells, *Trends Chem.*, 2022, **4**, 1005–1020.

92 Y. Lin, Y. Bai, Y. Fang, Z. Chen, S. Yang, X. Zheng, S. Tang, Y. Liu, J. Zhao and J. Huang, Enhanced Thermal Stability in Perovskite Solar Cells by Assembling 2D/3D Stacking Structures, *J. Phys. Chem. Lett.*, 2018, **9**, 654–658.

93 S. Sidhik, Y. Wang, M. De Siena, R. Asadpour, A. J. Torma, T. Terlier, K. Ho, W. Li, A. B. Puthirath, X. Shuai, A. Agrawal, B. Traore, M. Jones, R. Giridharagopal, P. M. Ajayan, J. Strzalka, D. S. Ginger, C. Katan, M. A. Alam, J. Even, M. G. Kanatzidis and A. D. Mohite, Deterministic fabrication of 3D/2D perovskite bilayer stacks for durable and efficient solar cells, *Science*, 2022, **377**, 1425–1430.

94 D. Zhang, X. Wang, Z. Fan, X. Xia and F. Li, Nondestructive Post-Treatment Enabled by In Situ Generated 2D Perovskites Derived from Multi-ammonium Molecule Vapor for High-Performance 2D/3D Bilayer Perovskite Solar Cells, *ACS Appl. Mater. Interfaces*, 2022, **14**, 51053–51065.

95 C. Deng, J. Wu, Y. Du, Q. Chen, Z. Song, G. Li, X. Wang, J. Lin, W. Sun, M. Huang, Y. Huang, P. Gao and Z. Lan, Surface Reconstruction and In Situ Formation of 2D Layer for Efficient and Stable 2D/3D Perovskite Solar Cells, *Small Methods*, 2021, **5**, e2101000.

96 X. Wang, Y. Wang, T. Zhang, X. Liu and Y. Zhao, Steric Mixed-Cation 2D Perovskite as a Methylammonium Locker to Stabilize MAPbI(3), *Angew. Chem., Int. Ed.*, 2020, **59**, 1469–1473.

97 W. Fan, Y. Shen, K. Deng, Q. Chen and Y. Bai, A tailored spacer molecule in 2D/3D heterojunction for ultralow-voltage-loss and stable perovskite solar cells, *J. Mater. Chem. A*, 2021, **9**, 26829–26838.

98 X. Yue, X. Zhao, B. Fan, Y. Yang, L. Yan, S. Qu, H. Huang, Q. Zhang, H. Yan, P. Cui, J. Ji, J. Ma and M. Li, Surface Regulation through Dipolar Molecule Boosting the Efficiency of Mixed 2D/3D Perovskite Solar Cell to 24%, *Adv. Funct. Mater.*, 2022, **33**, 2209921.

99 Yukta, N. Parikh, R. D. Chavan, P. Yadav, M. K. Nazeeruddin and S. Satapathi, Highly Efficient and Stable 2D Dion Jacobson/3D Perovskite Heterojunction Solar Cells, *ACS Appl. Mater. Interfaces*, 2022, **14**, 29744–29753.

100 S. J. Sung, J. Im, G. Kim, C. S. Moon, J. J. Yoo, S. S. Shin, N. J. Jeon, B. S. Ma, D. J. Kim, T. S. Kim and J. Seo, Molecular Engineering for Function-Tailored Interface Modifier in High-Performance Perovskite Solar Cells, *Adv. Energy Mater.*, 2022, **12**, 2200758.

101 G. Li, J. Song, J. Wu, Y. Xu, C. Deng, Z. Song, X. Wang, Y. Du, Q. Chen, R. Li, W. Sun and Z. Lan, Surface defect passivation by 1,8-Naphthyridine for efficient and stable Formamidinium-based 2D/3D perovskite solar cells, *Chem. Eng. J.*, 2022, **449**, 137806.

102 Y. Lv, X. Song, Y. Yin, Y. Feng, H. Ma, C. Hao, S. Jin and Y. Shi, Hexylammonium Iodide Derived Two-Dimensional Perovskite as Interfacial Passivation Layer in Efficient Two-Dimensional/Three-Dimensional Perovskite Solar Cells, *ACS Appl. Mater. Interfaces*, 2020, **12**, 698–705.

103 M. Singh, I. H. Ho, A. Singh, C.-W. Chan, J.-W. Yang, T.-F. Guo, H. Ahn, V. Tung, C. W. Chu and Y.-J. Lu, Unveiling Ultrafast Carrier Extraction in Highly Efficient 2D/3D Bilayer Perovskite Solar Cells, *ACS Photonics*, 2022, **9**, 3584–3591.

104 B. Zhang, D. Gao, M. Li, X. Shang, Y. Li, C. Chen and T. Pauporte, Heterojunction In Situ Constructed by a Novel Amino Acid-Based Organic Spacer for Efficient and Stable Perovskite Solar Cells, *ACS Appl. Mater. Interfaces*, 2022, **14**, 40902–40912.

105 T. Ye, A. Bruno, G. Han, T. M. Koh, J. Li, N. F. Jamaludin, C. Soci, S. G. Mhaisalkar and W. L. Leong, Efficient and Ambient-Air-Stable Solar Cell with Highly Oriented 2D@3D Perovskites, *Adv. Funct. Mater.*, 2018, **28**, 1801654.

106 K. T. Cho, Y. Zhang, S. Orlandi, M. Cavazzini, I. Zimmermann, A. Lesch, N. Tabet, G. Pozzi, G. Grancini and M. K. Nazeeruddin, Water-Repellent Low-Dimensional Fluorous Perovskite as Interfacial Coating for 20% Efficient Solar Cells, *Nano Lett.*, 2018, **18**, 5467–5474.

107 Q. He, M. Worku, L. Xu, C. Zhou, H. Lin, A. J. Robb, K. Hanson, Y. Xin and B. Ma, Facile Formation of 2D-3D Heterojunctions on Perovskite Thin Film Surfaces for Efficient Solar Cells, *ACS Appl. Mater. Interfaces*, 2020, **12**, 1159–1168.

108 Y. Huang, K. Yan, B. Niu, Z. Chen, E. Gu, H. Liu, B. Yan, J. Yao, H. Zhu, H. Chen and C.-Z. Li, Finite perovskite hierarchical structures via ligand confinement leading to efficient inverted perovskite solar cells, *Energy Environ. Sci.*, 2023, **16**, 557–564.

109 X. Jiang, J. Zhang, S. Ahmad, D. Tu, X. Liu, G. Jia, X. Guo and C. Li, Dion-Jacobson 2D-3D perovskite solar cells with improved efficiency and stability, *Nano Energy*, 2020, **75**, 104892.

110 Y. Yu, R. Liu, M. Xu and H. Yu, Diammonium-induced Dion-Jacobson 2D/3D wide-bandgap perovskite solar cells with enhanced efficiency and stability, *EcoMat*, 2022, **5**, e12272.

111 G. Li, J. Song, J. Wu, Z. Song, X. Wang, W. Sun, L. Fan, J. Lin, M. Huang, Z. Lan and P. Gao, Efficient and Stable 2D@3D/2D Perovskite Solar Cells Based on Dual Optimization of Grain Boundary and Interface, *ACS Energy Lett.*, 2021, **6**, 3614–3623.

112 J. Guo, B. Wang, D. Lu, T. Wang, T. Liu, R. Wang, X. Dong, T. Zhou, N. Zheng, Q. Fu, Z. Xie, X. Wan, G. Xing, Y. Chen and Y. Liu, Ultralong Carrier Lifetime Exceeding 20 micros in Lead Halide Perovskite Film Enable Efficient Solar Cells, *Adv. Mater.*, 2023, e2212126.

113 G. Yang, Z. Ren, K. Liu, M. Qin, W. Deng, H. Zhang, H. Wang, J. Liang, F. Ye, Q. Liang, H. Yin, Y. Chen, Y. Zhuang, S. Li, B. Gao, J. Wang, T. Shi, X. Wang, X. Lu, H. Wu, J. Hou, D. Lei, S. K. So, Y. Yang, G. Fang and G. Li, Stable and low-photovoltage-loss perovskite solar cells by multifunctional passivation, *Nat. Photonics*, 2021, **15**, 681–689.

114 T. Zhao, C.-C. Chueh, Q. Chen, A. Rajagopal and A. K. Y. Jen, Defect Passivation of Organic–Inorganic Hybrid Perovskites by Diammonium Iodide toward High-Performance Photovoltaic Devices, *ACS Energy Lett.*, 2016, **1**, 757–763.

115 B. B. Yu, Z. Chen, Y. Zhu, Y. Wang, B. Han, G. Chen, X. Zhang, Z. Du and Z. He, Heterogeneous 2D/3D Tin-Halides Perovskite Solar Cells with Certified Conversion Efficiency Breaking 14, *Adv. Mater.*, 2021, **33**, e2102055.

116 L. Iagher and L. Etgar, Effect of Cs on the Stability and Photovoltaic Performance of 2D/3D Perovskite-Based Solar Cells, *ACS Energy Lett.*, 2018, **3**, 366–372.

117 S.-H. Lee, S. Jeong, S. Seo, H. Shin, C. Ma and N.-G. Park, Acid Dissociation Constant: A Criterion for Selecting Passivation Agents in Perovskite Solar Cells, *ACS Energy Lett.*, 2021, 1612–1621.

118 S. Jeong, S. Seo, H. Yang, H. Park, S. Shin, H. Ahn, D. Lee, J. H. Park, N. G. Park and H. Shin, Cyclohexylammonium-Based 2D/3D Perovskite Heterojunction with Funnel-Like Energy Band Alignment for Efficient Solar Cells (23.91%), *Adv. Energy Mater.*, 2021, **11**, 2102236.

119 S. Wang, F. Cao, P. Chen, R. He, A. Tong, Z. Lan, P. Gao, W. Sun and J. Wu, Two birds with one stone: Simultaneous realization of constructed 3D/2D heterojunction and p-doping of hole transport layer for highly efficient and stable perovskite solar cells, *Chem. Eng. J.*, 2023, **453**, 139721.

120 Y. Du, J. Wu, G. Li, X. Wang, Z. Song, C. Deng, Q. Chen, Y. Zou, W. Sun and Z. Lan, Bulky ammonium iodide and in-situ formed 2D Ruddlesden-Popper layer enhances the stability and efficiency of perovskite solar cells, *J. Colloid Interface Sci.*, 2022, **614**, 247–255.

121 H. Ju, Y. Ma, Y. Cao, Z. Wang, L. Liu, M. Wan, T. Mahmoudi, Y.-B. Hahn, Y. Wang and Y. Mai, Roles of Long-Chain Alkylamine Ligands in Triple-Halide Perovskites for Efficient NiOx-Based Inverted Perovskite Solar Cells, *Solar RRL*, 2022, **6**, 2101082.

122 J. Sun, X. Zhang, X. Ling, Y. Yang, Y. Wang, J. Guo, S. Liu, J. Yuan and W. Ma, A penetrated 2D/3D hybrid heterojunction for high-performance perovskite solar cells, *J. Mater. Chem. A*, 2021, **9**, 23019–23027.

123 M. A. Mahmud, H. T. Pham, T. Duong, Y. Yin, J. Peng, Y. Wu, W. Liang, L. Li, A. Kumar, H. Shen, D. Walter, H. T. Nguyen, N. Mozaffari, G. D. Tabi, G. Andersson, K. R. Catchpole, K. J. Weber and T. P. White, Combined Bulk and Surface Passivation in Dimensionally Engineered 2D-3D Perovskite Films via Chlorine Diffusion, *Adv. Funct. Mater.*, 2021, **31**, 2104251.

124 M. Dehghanipour, A. Behjat and H. Amrollahi Bioki, Fabrication of stable and efficient 2D/3D perovskite solar cells through post-treatment with TBABF4, *J. Mater. Chem. C*, 2021, **9**, 957–966.

125 H. Xu, G. Liu, X. Xu, S. Xu, L. Zhang, X. Chen, H. Zheng and X. Pan, Hydrophobic 2D Perovskite-Modified Layer with Polyfunctional Groups for Enhanced Performance and High Moisture Stability of Perovskite Solar Cells, *Solar RRL*, 2020, **4**, 2000647.

126 X. Zhang, W. Zhou, X. Chen, Y. Chen, X. Li, M. Wang, Y. Zhou, H. Yan, Z. Zheng and Y. Zhang, Dual Optimization of Bulk and Surface via Guanidine Halide for Efficient and Stable 2D/3D Hybrid Perovskite Solar Cells, *Adv. Energy Mater.*, 2022, **12**, 2201105.

127 B. Liu, J. Hu, D. He, L. Bai, Q. Zhou, W. Wang, C. Xu, Q. Song, D. Lee, P. Zhao, F. Hao, X. Niu, Z. Zang and

J. Chen, Simultaneous Passivation of Bulk and Interface Defects with Gradient 2D/3D Heterojunction Engineering for Efficient and Stable Perovskite Solar Cells, *ACS Appl. Mater. Interfaces*, 2022, **14**, 21079–21088.

128 C. Ge, Y. Z. B. Xue, L. Li, B. Tang and H. Hu, Recent Progress in 2D/3D Multidimensional Metal Halide Perovskites Solar Cells, *Front. Mater.*, 2020, **7**, 601179.

129 W. Gao, H. Dong, N. Sun, L. Chao, W. Hui, Q. Wei, H. Li, Y. Xia, X. Gao, G. Xing, Z. Wu, L. Song, P. Müller-Buschbaum, C. Ran and Y. Chen, Chiral cation promoted interfacial charge extraction for efficient tin-based perovskite solar cells, *J. Energy Chem.*, 2022, **68**, 789–796.

130 M. A. Mahmud, T. Duong, Y. Yin, H. T. Pham, D. Walter, J. Peng, Y. Wu, L. Li, H. Shen, N. Wu, N. Mozaffari, G. Andersson, K. R. Catchpole, K. J. Weber and T. P. White, Double-Sided Surface Passivation of 3D Perovskite Film for High-Efficiency Mixed-Dimensional Perovskite Solar Cells, *Adv. Funct. Mater.*, 2019, **30**, 1907962.